

HPr prevents FruR-mediated facilitation of RNA polymerase binding to the *fru* promoter in *Vibrio cholerae*

Chang-Kyu Yoon^{1,2,†}, Seung-Hwan Lee^{1,†}, Jing Zhang^{3,†}, Hye-Young Lee^{1,2},
Min-Kyu Kim^{1,3,*} and Yeong-Jae Seok^{1,*}

¹School of Biological Sciences and Institute of Microbiology, Seoul National University, Seoul, 08826, Korea,

²Research Institute of Basic Science, Seoul National University, Seoul, 08826, Korea and ³Advanced Radiation Technology Institute, Korea Atomic Energy Research Institute, Jeongseup, 56212, Korea

Received September 30, 2022; Revised February 17, 2023; Editorial Decision March 10, 2023; Accepted March 15, 2023

ABSTRACT

Phosphorylation state-dependent interactions of the phosphoenolpyruvate (PEP):carbohydrate phosphotransferase system (PTS) components with transcription factors play a key role in carbon catabolite repression (CCR) by glucose in bacteria. Glucose inhibits the PTS-dependent transport of fructose and is preferred over fructose in *Vibrio cholerae*, but the mechanism is unknown. We have recently shown that, contrary to *Escherichia coli*, the fructose-dependent transcriptional regulator FruR acts as an activator of the *fru* operon in *V. cholerae* and binding of the FruR–fructose 1-phosphate (F1P) complex to an operator facilitates RNA polymerase (RNAP) binding to the *fru* promoter. Here we show that, in the presence of glucose, dephosphorylated HPr, a general PTS component, binds to FruR. Whereas HPr does not affect DNA-binding affinity of FruR, regardless of the presence of F1P, it prevents the FruR–F1P complex from facilitating the binding of RNAP to the *fru* promoter. Structural and biochemical analyses of the FruR–HPr complex identify key residues responsible for the *V. cholerae*-specific FruR–HPr interaction not observed in *E. coli*. Finally, we reveal how the dephosphorylated HPr interacts with FruR in *V. cholerae*, whereas the phosphorylated HPr binds to CcpA, which is a global regulator of CCR in *Bacillus subtilis* and shows structural similarity to FruR.

INTRODUCTION

To ensure the sequential utilization of carbohydrates in the environment, most bacteria promote the expression or activity of enzymes and transporters required for the metabolism of a preferred carbohydrate while simultaneously inhibiting the expression or activity of those specific to other carbohydrates. This regulatory mechanism is called carbon catabolite repression (CCR) (1).

Carbohydrates transported by the phosphoenolpyruvate (PEP):carbohydrate phosphotransferase system (PTS) are usually preferred over those transported by non-PTS (1–3). The PTS comprises two general components: enzyme I (EI) and histidine phosphocarrier protein (HPr), which are required for the phosphorylation of most PTS sugars and various carbohydrate-specific EII components (1–3). As the PTS components transfer the phosphoryl group derived from PEP to the transported carbohydrate sequentially, their phosphorylation status reflects the availability of the PTS sugar.

Besides sugar transport, these PTS components interact with other proteins in a phosphorylation state-dependent manner to regulate bacterial physiology (2). In particular, the interaction of PTS components with transcription factors that regulate the expression of genes involved in the utilization of carbohydrates in a phosphorylation-dependent manner is one of the key factors in the CCR mechanism (1,3–5). In *Escherichia coli*, in the presence of glucose, dephosphorylated HPr binds to the mannitol repressor (MtlR) and represses the transcription of the *mtl* operon, which encodes a mannitol-specific PTS, mannitol 6-phosphate dehydrogenase and MtlR itself (6,7). However, when glucose is depleted, the ratio of phosphorylated HPr that cannot interact with MtlR increases, resulting in the

*To whom correspondence should be addressed. Tel: +82 2 880 4414; Fax: +82 2 871 1993; Email: yjseok@snu.ac.kr

Correspondence may also be addressed to Min-Kyu Kim. Tel: +82 63 570 3212; Email: mkkim@kaeri.re.kr

[†]The authors wish it to be known that, in their opinion, the first three authors should be regarded as Joint First Authors.

Present address: Jing Zhang, The Center for Microbes, Development and Health, CAS Key Laboratory of Molecular Virology and Immunology, Institute Pasteur of Shanghai, Chinese Academy of Sciences, Shanghai, 200031, China.

derepression of the *mtl* operon, facilitating the transport and catabolism of mannitol. Furthermore, in the absence of glucose, the phosphorylated form of EIIA^{Glc} increases and stimulates the activity of adenylate cyclase, an enzyme that converts ATP to cyclic AMP (cAMP) (8). The cAMP receptor protein (CRP)-cAMP complex activates the transcription of genes that encode enzymes and transporters involved in the use of less favoured carbohydrates (4). In Firmicutes, ATP-dependent phosphorylation of HPr on the Ser46 residue by bifunctional HPr kinase/phosphorylase (HPrK/P) plays a central role in CCR by binding to the global transcriptional regulator carbon catabolite protein A (CcpA) (3,9–10).

Vibrio species also recognize carbohydrates present in the habitat and host environment through the PTS and regulate their physiology through the protein-protein interaction of the PTS proteins (11–20). Several lines of evidence have demonstrated that the transcriptional level of genes encoding the fructose PTS (PTS^{Fru}) increases during host infection in *Vibrio* species (21–23) and that utilization of fructose through the PTS is essential for the intestinal colonization of *Vibrio cholerae* (24). To understand this, we recently established the molecular mechanism of the fructose regulator (FruR)-mediated transcriptional activation of the fructose operon (*fru* operon), which contains genes encoding PTS^{Fru} components in *V. cholerae* (18). Fructose is transported via the PTS and is concomitantly phosphorylated to fructose 1-phosphate (F1P). In the presence of fructose, the FruR-F1P complex binds directly to the operator located between the –35 and –10 promoter elements of the *fru* promoter and induces DNA structural modifications, facilitating the binding of RNA polymerase (RNAP) to the promoter DNA. Glucose inhibits the PTS-mediated transport and phosphorylation of fructose and therefore is preferred over fructose in *V. cholerae*. However, the underlying molecular mechanism remains unknown (25).

Here, we reveal that, in the presence of glucose, dephosphorylated HPr inhibits the FruR-mediated facilitation of the binding of RNAP to the *fru* promoter without affecting the binding affinity of FruR to DNA or F1P. In addition, the crystal structure of the FruR-HPr complex reveals a distinct binding mode of HPr to the GalR-LacI family transcription factor in *V. cholerae*, compared to *Bacillus subtilis*, and explains why this interaction is not observed in *E. coli*.

MATERIALS AND METHODS

Bacterial strains, plasmids and culture conditions

Details of the strains, plasmids, and oligonucleotides used in this study are listed in Supplementary Tables 1 and 2. All *V. cholerae* N16961 strains were cultured in Luria-Bertani (LB) medium or M9 minimal medium supplemented with the indicated sugars at 37°C. All *E. coli* strains were grown in LB medium at 37°C. All plasmids were constructed using standard PCR-based cloning procedures and verified by sequencing. A *V. cholerae ptsH* mutant was generated by deleting the DNA region from +22 to +230 relative to the initiation codon of *ptsH* using pDM4 vector-based recombination, as previously described (26). Protein expression plasmids were constructed as previously described (18). Amino acid substitution mutants of FruR and HPr were

generated by site-directed mutagenesis PCR using the appropriate primer pairs (Supplementary Table S2).

Determination of the amount of sugar in the culture medium

The amount of sugar in the bacterial culture medium was determined as previously described (6). Overnight-grown *V. cholerae* N16961 cells were inoculated in M9 minimal medium containing glucose and fructose. Aliquots (1 ml) were withdrawn at the indicated incubation times to determine residual sugars in the culture medium. After centrifugation at 10 000 × *g* for 2 min, the sugars remaining in the culture supernatant were analysed using a Sugar-Pak I column connected to a Dionex Ultimate 3000 high-performance liquid chromatography system equipped with a refractive index detector (Thermo Fisher Scientific, Inc., Waltham, MA, USA). Distilled water was used as the mobile phase, and the column was maintained at 75°C during the experiment.

RNA extraction and quantitative real-time reverse transcription PCR (qRT-PCR)

RNA extraction and qRT-PCR were performed as previously described (18). After fixing cells with the same volume of 100% methanol for 1 h at –20°C, total RNA was isolated using the TaKaRa MiniBEST Universal RNA Extraction Kit (Takara Bio, Inc., Otsu, Japan, #9767) following the manufacturer's instructions. Total RNA (2500 ng) from each sample was converted to cDNA using the RNA to cDNA EcoDry Premix (Random Hexamers) (Clontech Laboratories, Inc., Mountain View, CA, USA, #639545). Twenty-fold diluted cDNA was subjected to real-time PCR amplification using FAST SYBRTM Green Master Mix (Thermo Fisher Scientific, Inc., Waltham, MA, USA, #4385616) with specific primers (Supplementary Table S2) in a CFX96TM Real-Time System (BioRad, Hercules, CA, USA).

Purification of proteins

His-tagged proteins were overexpressed in *E. coli* ER2566 or BL21/pLysSRARE and purified by immobilized metal affinity chromatography (IMAC) using TALON metal affinity resin following the manufacturer's instructions (Clontech Laboratories, Inc., Mountain View, CA, USA). The harvested cells were resuspended in buffer A (50 mM Tris-HCl, pH 8.0; 200 mM NaCl; 5 mM β-mercaptoethanol; and 10% glycerol) and disrupted by three passages through a French pressure cell at 9000 psi. The proteins bound to the resin were washed with buffer A containing 10 mM imidazole (buffer B) and eluted with buffer A containing 200 mM imidazole (buffer C). To remove imidazole and achieve higher purity (>98%), concentrated proteins were subjected to further chromatography using a HiLoad 16/600 Superdex 200 prep grade column (GE Healthcare Life Sciences, Chicago, IL, USA) equilibrated with buffer A (18).

Protein ligand-fishing experiment

Wild-type (WT) *V. cholerae* cells (400 ml) were resuspended in buffer A and disrupted by three passages through a

French pressure cell at 9000 psi. After centrifugation at $10\,000 \times g$ for 20 min at 4°C, the supernatant was divided into two aliquots, mixed with 250 µg His-tagged protein as bait or buffer A as a control and then incubated for 20 min at 4°C. When His-tagged HPr was used as bait, HPr was dephosphorylated by adding 2 mM pyruvate or phosphorylated by adding 2 mM PEP to the mixture (12,16). After a brief wash with buffer B, the bound proteins were eluted with buffer C and then analysed on a 4–20% gradient polyacrylamide gel (acrylamide/bisacrylamide ratio of 37.5:1) (KOMA biotech, Seoul, Korea, KG8531) in Tris-glycine buffer (25 mM Tris; 192 mM glycine) supplemented with 0.1% SDS followed by staining with Coomassie Brilliant Blue R. After the protein bands specifically bound to the His-tagged bait protein were excised from the gel, in-gel digestion and peptide mapping of the tryptic digests were performed using MALDI-TOF MS.

Protein binding assay using native polyacrylamide gel electrophoresis (native PAGE)

To examine the phosphorylation state-dependent binding of HPr to FruR, 2 µg of HPr and 8 µg of FruR were incubated with 1 µg of EI and 2 mM PEP or 2 mM pyruvate in buffer P (10 mM sodium phosphate, pH 8.0; 2 mM MgCl₂; 1 mM EDTA; 10 mM KCl; and 5 mM DTT) for 10 min at 37°C (27). The reaction mixtures were resolved on a 4–20% gradient polyacrylamide gel (SDS-PAGE) or 10% polyacrylamide gel (native PAGE) in Tris-glycine buffer supplemented with or without 0.1% SDS, respectively, and then stained with Coomassie Brilliant Blue R (28).

Determination of the *in vivo* phosphorylation state of HPr

The phosphorylation state of HPr was determined as previously described with minor modifications (28). Overnight-grown *V. cholerae* N16961 cultures were diluted 100-fold to fresh LB medium containing indicated sugars and cultured at 37°C until the OD₆₀₀ reached 1.0. Cultured cells (200 µl) were quenched, the phosphorylation states of HPr were fixed, and the cells were simultaneously disrupted by mixing with 20 µl 5 M NaOH, followed by vortexing for 10 s. After adding 80 µl of 3 M sodium acetate (pH 5.2) and 900 µl ethanol, the samples were incubated at –80°C for 10 min, followed by centrifugation at $10\,000 \times g$ at 4°C for 10 min. The pellets were suspended in 20 µl native PAGE sample buffer (72 mM Tris-HCl, pH 6.8; 30% glycerol; 17.3 mM β-mercaptoethanol; 0.1% bromophenol blue) containing 1 M urea and subjected to native PAGE on a 10% polyacrylamide gel and western blotting (28). Protein amounts were normalized to the cell density.

Electrophoretic mobility shift assay (EMSA)

A 338-bp probe covering the entire *fruR*–*fruB* intergenic region was prepared by PCR (18) and incubated with the indicated proteins and fructose 1-phosphate (F1P) (Santa Cruz Biotechnology, Dallas, TX, USA, #sc-285345) in TGED buffer (10 mM Tris-HCl, pH 8.0; 5% v/v glycerol; 0.1 mM EDTA and 1 mM DTT). Bovine serum albumin (BSA, 200 µg/ml) was used as a non-specific protein competitor. Each

sample was incubated at 37°C for 10 min and then analysed on a 6% polyacrylamide gel (acrylamide/bisacrylamide ratio of 29:1) in TBE (89 mM Tris, 89 mM boric acid, 2 mM EDTA) followed by EtBr staining. DNA bands were visualised using a gel documentation system (GDS-200C, KBT, Seongnam, Korea), and their intensities were quantified using ImageJ software (NIH Image, National Institutes of Health, Bethesda, MD, USA; online at: <http://rsbweb.nih.gov/ij/>).

DNase I footprinting

DNase I footprinting assay was performed as previously described (29). The 6-carboxyfluorescein (6' FAM)-labelled 538-bp *fruB* probe covering from –199 to +339 bp relative to the transcription start site (TSS) was prepared by PCR (18). The purified PCR product was incubated with the indicated amounts of proteins at 37°C for 10 min before digestion with 0.02 U DNase I (New England Biolabs, Beverly, MA, USA, # M0303S) for 1 min. The cleavage reaction was stopped by adding the same volume of stop solution (200 mM NaCl, 30 mM EDTA, 1% SDS), followed by phenol extraction and EtOH precipitation. DNase I digestion reactions were analysed by capillary electrophoresis in an ABI 3730xl DNA Analyzer (Applied Biosystems, Foster City, CA, USA) with Peak Scanner software v1.0 (Applied Biosystems, Foster City, CA, USA).

In vitro transcription assay

In vitro transcription assays were performed as previously described with minor modifications (30,31). Briefly, a 418-bp template DNA spanning from –99 to +319 bp relative to the TSS was prepared by PCR from pSA-PfruB (Supplementary Table S1) using primers, PfruB-IVT-F1 and PfruB-IVT-R1 (Supplementary Table S2). The template DNA (1 µg) was incubated with 1 µg FruR in the presence or absence of 1 mM F1P or 1 µg HPr for 10 min at 37°C in a 36 µl reaction mixture containing RNA polymerase reaction buffer (New England Biolabs, Beverly, MA, USA, #M0550S). The mixture was supplemented with a mixture of nucleotide triphosphate (NTP) (0.5 mM each NTP) (Invitrogen, Carlsbad, CA, USA, #18109017), 40 units of RNaseOUT™ (Invitrogen, Carlsbad, CA, USA, #10777019) and purified *V. cholerae* RNAP proteins (RpoA, RpoB, RpoC, and RpoZ; 0.49, 0.13, 0.13, and 1.35 µM, respectively) saturated with 0.26 µM *V. cholerae* σ⁷⁰, and incubated for 1 h at 37°C. The DNA templates were digested with 1 unit of DNase I (New England Biolabs, Beverly, MA, USA, # M0303S) for 30 min at 37°C, followed by RNA extraction with acid phenol-chloroform (5:1, pH 4.5, Ambiofn, Austin, TX, USA, #AM9722) and EtOH precipitation. The purified RNA (5 µl) was annealed with 30 pmol hexachlorofluorescein (HEX) labelled primer fruB-IVT-R2, which anneals the region from +92 to +112 relative to the TSS (Supplementary Table S2), and then extended using 5 units of AMV reverse transcriptase (Promega, Madison, WI, USA, #M5101) for 1 h at 42°C following the manufacturer's instructions. A 133-bp HEX-labelled DNA prepared with unlabelled PfruB-IVT-F2 and HEX-labelled PfruB-

IVT-R2 (Supplementary Table S2) was added to each sample to a final concentration of 0.1 ng/ μ l. The samples were analysed using an ABI 3730xl DNA analyzer (Applied Biosystems, Foster City, CA, USA) with Peak Scanner software v1.0 (Applied Biosystems, Foster City, CA, USA).

Isothermal titration calorimetry (ITC)

The samples for the isothermal titration calorimetry (ITC) experiments were extensively dialysed (two changes, >24 h total) against the ITC binding buffer [20 mM potassium phosphate, pH 8.0; 100 mM NaCl; 5 mM tris(2-carboxyethyl)phosphine] using SnakeSkin™ Dialysis Tubing with a molecular weight cut-off of 3.5 kDa (Thermo Fisher Scientific, Inc., Waltham, MA, USA, #68035). After dialysis, protein concentration was determined by ultraviolet absorbance at 280 nm. For titrations, samples were loaded into a 96-deep-well plate (Malvern Panalytical, Worcestershire, UK, #WEL020854-010) with three consecutive wells filled for a single titration: samples for the reaction cell, the injection syringe and the binding buffer for pre-rinsing the reaction cell (32,33). The fourth plate well was used to recover the reaction mixture after each titration for visual inspection of potential aggregation. All titrations were performed at 25°C using an automated MicroCal AutoPEAQ ITC instrument (Malvern Panalytical, Worcestershire, UK). The mean enthalpies measured from the injection of the ligands into the buffer were subtracted from the raw titration data before data fitting using MicroCal software. From the curves, parameters ΔH (reaction enthalpy) and K_d (binding constant) were determined.

Crystallization, data collection and structure determination of the FruR–HPr complex

Crystals of the FruR–HPr complex were grown using the vapor batch crystallization method (34) at 22°C by mixing equal volumes (1 μ l each) of the protein solution (at 13 mg/ml concentration) and the reservoir solution comprising 0.2 M calcium acetate, 30% (w/v) PEG 3350 and 10 μ M spermidine. For data collection, FruR–HPr complex crystals were mounted using a 75 mm MicroMount polymer loop (MiTeGen, Ithaca, NY, USA) and cooled to 100 K using a Cryostream cooler (Oxford Cryosystems, Oxford, UK). A 2.0 Å resolution native data set was collected at a wavelength of 0.97934 Å using an ADSC Quantum 315r CCD detector (ADSC, Poway, CA, USA) at beamline BL-7A of the Pohang Light Source, Republic of Korea. The diffraction data were processed and scaled using DENZO and SCALEPACK from the HKL-2000 program suite (35). Crystals of FruR–HPr complex belonged to the primitive orthorhombic space group $P2_12_12_1$, with unit cell parameters of $a = 33.94$ Å, $b = 62.36$ Å, $c = 312.67$ Å and $\alpha = \beta = \gamma = 90.00^\circ$.

The structure of the FruR–HPr complex was solved by the molecular replacement phasing method using the structures of CcpA and HPr of *Priestia megaterium* (PDB code: 1RZR) (36) as search models using the Phaser program in the PHENIX program suite (37). Further model building was completed using Coot (38) and refinement was performed using phenix.refine in the PHENIX program suite.

The final refinement resulted in R_{work} of 18.09% and R_{free} of 22.06%. The figures showing the structures were prepared using PyMOL (<https://pymol.org>). Data collection and refinement statistics are summarized in Supplementary Table S3.

RESULTS

Glucose inhibits fructose-dependent transcriptional activation of the fru operon in *Vibrio cholerae*

Vibrio cholerae prefers glucose over fructose and therefore exhibits diauxic growth in a minimal medium supplemented with glucose and fructose (25). Furthermore, glucose inhibits PTS-dependent transport and phosphorylation of fructose by approximately 87% and 82%, respectively (25). To determine the mechanism underlying the preferential utilization of glucose over fructose, we measured the growth of wild-type (WT) *V. cholerae* N16961 cells in a minimal medium supplemented with glucose and fructose and measured the amount of sugar remaining in the medium. As expected, WT *V. cholerae* N16961 exhibited a typical diauxic growth curve, and fructose consumption was hardly detected in the first growth phase, during which glucose was consumed (Figure 1A).

The sequential utilization of sugars is usually accompanied by the inhibition of genes encoding proteins involved in the metabolism and transport of unfavourable sugars (3). Therefore, we assumed that the transcription of the fru operon, which contains genes encoding PTS^{Fru} components (FruB and FruA) and 1-phosphofruktokinase (FruK), could be inhibited in response to the presence of glucose (39). In a previous study, we revealed that fructose-dependent transcriptional activation of the fru operon in *V. cholerae* was mediated primarily by the transcription activator FruR (18). Therefore, we measured the transcription levels of fruR and fruB at several time points on the growth curve. Similarly to a previous study on the preference between glucose and mannitol in *E. coli* (6), the transcription of fruB and fruR increased significantly after the diauxic shift, indicating that glucose inhibits the inductive effect of fructose on the transcription of the fru operon and fruR (Figure 1B).

FruR directly binds to dephosphorylated HPr

Because FruR acts as a transcriptional activator in the presence of fructose and presumably as a weak transcriptional repressor in the absence of fructose in *V. cholerae* (18,40), we speculated that other factors may be involved in the transcriptional inhibition of the fru operon in the presence of glucose. Furthermore, because the transcription of the fru operon is primarily regulated by FruR (18,41), we assumed this factor(s) might inhibit the transcription of the fru operon by regulating FruR activity through direct binding to FruR. To verify this assumption, we explored a new interacting protein of FruR through ligand-fishing experiments (6,16–17) using FruR tagged with His₆ at the C-terminus (FruR-His) as bait (Figure 2A). Total proteins extracted from WT *V. cholerae* N16961 cells grown in LB medium supplemented with 0.2% glucose were mixed with metal affinity resin in the presence or absence of purified

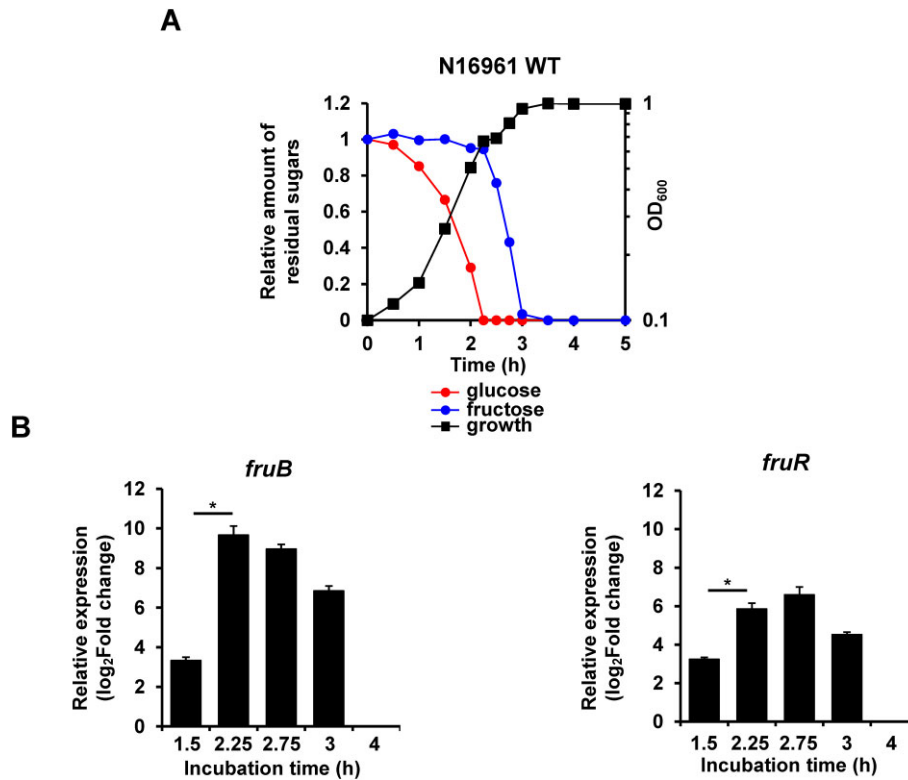


Figure 1. Glucose inhibits fructose-dependent transcriptional activation of the *fru* operon in *V. cholerae*. Wild-type (WT) *V. cholerae* N16961 cells were cultured in M9 medium supplemented with 0.04% glucose and 0.04% fructose. (A) The growth and concentration of sugars remaining in the medium were measured at the indicated incubation times. (B) Relative transcript levels of *fruB* (left panel) and *fruR* (right panel) in WT *V. cholerae* cells withdrawn at the indicated incubation times were quantified by qRT-PCR. The mRNA expression levels of genes are shown as relative values (log₂ scale) to those of the cells withdrawn at 4 h incubation time. The means and standard deviations of three independent measurements are shown in (B). Statistical significance was determined using the Student's *t*-test (**P* < 0.005).

FruR-His. In repeated experiments, we found an interacting protein with an apparent molecular mass of 10 kDa, only in the fraction containing FruR-His (Figure 2A, lane B). Through peptide mapping after in-gel tryptic digestion, this protein was revealed to be the general PTS component, HPr (VC0966). To confirm the specific interaction between FruR and HPr, we conducted a ligand-fishing experiment using hexahistidine-tagged HPr at the N-terminus (His-HPr) as bait with crude extract of WT cells cultured in an LB medium. We added 2 mM PEP or pyruvate to the mixture of HPr and the crude extract to phosphorylate or dephosphorylate HPr (Figure 2B, lanes P and D, respectively) and determined whether the interaction of HPr with FruR depends on the phosphorylation status of HPr (12). We identified three proteins that interact specifically with dephosphorylated HPr. In-gel tryptic digestion, MALDI-TOF MS, and peptide mass fingerprinting revealed a protein band migrating at ~55 kDa as pyruvate kinase PykA (VC0485), a band at ~36 kDa as FruR, and a band at ~35 kDa as PyrB (VC2510). PykA was previously shown to interact with dephosphorylated HPr in *Vibrio vulnificus* (12,15), indicating that the ligand-fishing method used in this study was reliable (16).

To further confirm the specificity of the interaction between dephosphorylated HPr and FruR, the binding of the two proteins was examined using native-gel PAGE (28). We incubated HPr with enzyme I (EI) and 2 mM PEP or pyru-

vate, mixed with FruR, divided into two aliquots, and subjected to SDS-PAGE (used as loading control) and native PAGE, respectively (Figure 2C). When the HPr/FruR mixture was loaded in the presence of pyruvate, the intensities of both HPr and FruR bands decreased with the concomitant appearance of a new band corresponding to the FruR-HPr complex (lanes 1, 3 and 6 in Figure 2C). As previously reported (28), HPr was phosphorylated by EI in the presence of PEP and migrated faster on a native-gel than dephosphorylated HPr (Figure 2C, lower panel, lane 5). Interestingly, the band of the FruR-HPr complex was not observed in the sample containing phosphorylated HPr or FruR (Figure 2C, lower panel lane 7).

To transport most PTS sugars, including glucose, the phosphate group derived from EI is transferred to sugar-specific EII complexes by HPr (1). However, when fructose is transported, FruB, which comprises an HPr-like domain (FPr) fused to an EIIA domain through a central M domain, transfers the phosphate group derived from EI to FruA (Figure 2D, upper panel) (39,42). According to previous studies, EIIA^{Glc} is mainly phosphorylated in cells grown on fructose (43), and the phosphorylation status of EIIA^{Glc} is like that of HPr (28). Therefore, we hypothesized that the ratio of phosphorylated HPr to total HPr proteins would be higher in fructose-grown *V. cholerae* cells than in glucose-grown cells. To verify this assumption, the phosphorylation state of HPr in cells grown on various PTS sugars

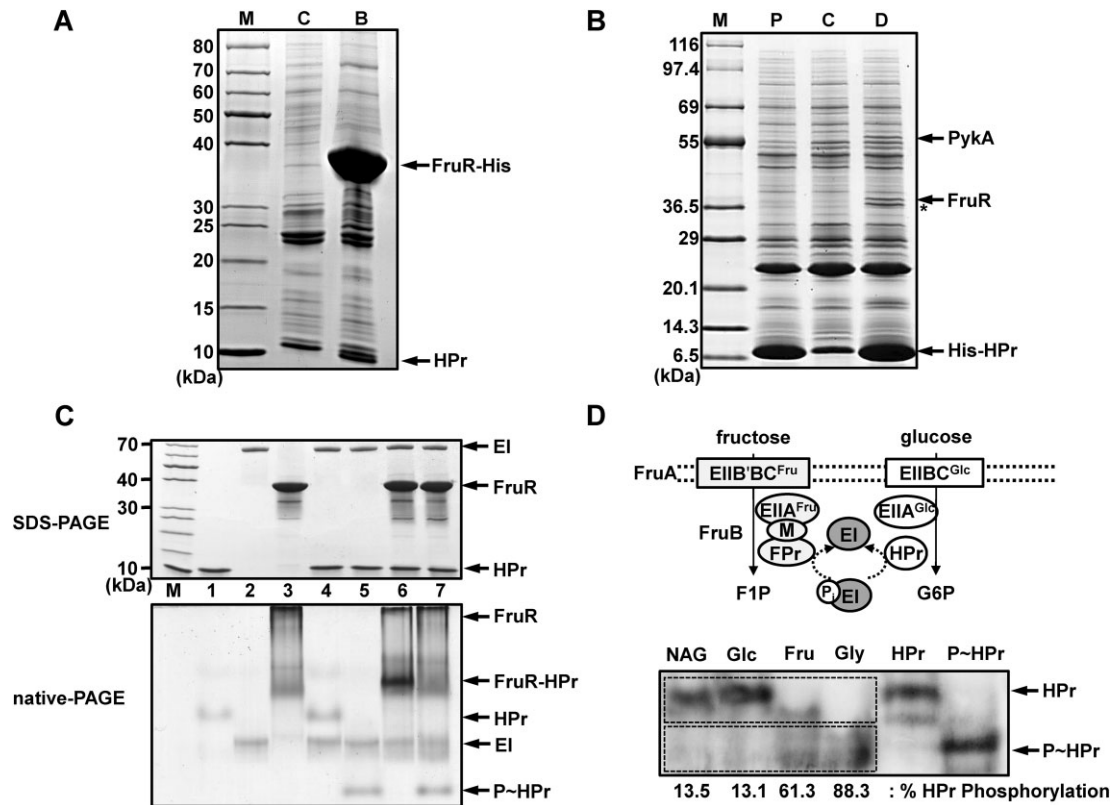


Figure 2. FruR directly binds to dephosphorylated HPr. (A) The ligand-fishing experiment was performed to find proteins that interact with FruR. The crude extract prepared from *V. cholerae* N16961 cells cultured in LB medium supplemented with 0.2% glucose was mixed with 250 μ g His-tagged FruR (lane B) or buffer (lane C) as a control. Each mixture was subjected to TALON metal affinity chromatography and proteins bound to the column were analysed. (B) The ligand-fishing experiment was performed using His-tagged HPr as bait or buffer as control (lane C) and mixed with crude extract prepared from *V. cholerae* N16961 cells cultured in LB medium. The extract containing His-HPr was supplemented with 2 mM PEP to phosphorylate HPr (lane P) or 2 mM pyruvate to dephosphorylate HPr (lane D). The protein band marked with an asterisk was identified as PyrB, which is not covered in this study. (C) To test the phosphorylation state-dependent binding of HPr to FruR, EI (1 μ g), HPr (2 μ g) and FruR (8 μ g) were incubated in different combinations in buffer P as indicated. Pyruvate (lanes 4 and 6) or PEP (lanes 5 and 7) was added to 2 mM. Each reaction mixture was incubated at 37°C for 10 min and then divided into two aliquots. One aliquot was analysed by SDS-PAGE (upper panel) to ensure the purity and the amount of each protein used in each reaction, and the other by native PAGE (lower panel) to measure the electrophoretic mobility shifts of HPr complexed with FruR. (D) The schematic representation of PTS-dependent fructose and glucose transport in *V. cholerae* (upper panel): F1P, fructose 1-phosphate; G6P, glucose 6-phosphate. The phosphorylation state of HPr was determined in *V. cholerae* N16961 cells grown in LB medium supplemented with 0.2% indicated carbon source (lower panel): Fru, fructose; Glc, glucose; Gly, glycerol; NAG, *N*-acetylglucosamine. Purified HPr (20 ng) was used as a positive control. Band intensities were analysed using ImageJ software. The percentage of phosphorylated HPr (lower rectangular) over total HPr is indicated below the gel.

(glucose, NAG, and fructose) and a non-PTS sugar (glycerol) was measured by western blotting using an antibody against *V. vulnificus* HPr (12). As expected, although HPr existed mostly in a dephosphorylated form in the presence of glucose or NAG, approximately 88% of HPr proteins were phosphorylated in the presence of glycerol (Figure 2D, lower panel) (6,28). Interestingly, more than half of HPr was phosphorylated in *V. cholerae* cells grown on fructose (Figure 2D, lower panel). In the presence of glucose, HPr is dephosphorylated and binds directly to FruR, whereas in the presence of fructose alone, HPr is mostly in the phosphorylated form that does not bind to FruR.

Dephosphorylated HPr regulates the FruR-mediated transcriptional activation of the *fru* promoter

Because FruR is required for the transcription of the *fru* operon in *V. cholerae* (18), we assumed that dephosphorylated HPr could affect the transcriptional activation of the *fru* promoter by binding to FruR. To examine whether

dephosphorylated HPr inhibits the transcriptional activation of the *fru* promoter, we transformed the *V. cholerae* N16961 *lacZ*⁻ strain carrying *E. coli lacZ* transcriptionally fused with the *V. cholerae fruB* promoter (P_{fruB}) (18) with a plasmid expressing a non-phosphorylatable form of HPr (pHPr(H15A)) or a plasmid expressing a phosphomimetic form of HPr (pHPr(H15D)) or an empty vector (EV) as control and measured the P_{fruB} activity in all strains grown either on glucose or fructose by measuring β -galactosidase activity. In the case of strains that harbour the plasmid carrying pHPr(H15D) or EV, cells grown on fructose exhibited significantly higher β -galactosidase activity than cells grown on glucose. However, the strain harbouring pHPr(H15A) exhibited no significant increase in β -galactosidase activity in the presence of fructose compared to that in the presence of glucose (Supplementary Figure S1).

In *V. cholerae*, FruR-mediated transcriptional activation of the *fru* operon is required for the growth on fructose (18). Thus, we assumed that the strain that harbours

pHPr(H15A) would exhibit growth retardation on fructose. To verify this assumption, we constructed the WT N16961 strain that harbours pHPr(WT) or pHPr(H15A) or pHPr(H15D), then examined the growth of each strain in a minimal medium containing 0.2% glucose or fructose. Although all strains showed growth rates similar to the WT strain harbouring an empty plasmid on glucose (Figure 3A, left panel), the WT strain carrying pHPr(H15A) showed severe growth defects on fructose, whereas the strain harbouring an expression vector for WT HPr or HPr(H15D) showed a similar growth rate as the strain harbouring an empty plasmid on fructose (Figure 3A, right panel). These data validated that dephosphorylated HPr directly binds to FruR and inhibits its transcriptional activation of the *fru* operon.

To further confirm that HPr inhibits FruR-mediated transcription of the *fru* operon, we performed *in vitro* transcription assays using the *V. cholerae* RNAP holoenzyme and FruR in the presence or absence of F1P or HPr (Figure 3B). The 112-bp *fruB* transcript was detected at a low level in the transcription reaction in the absence of FruR, HPr and F1P (control). The addition of FruR was insufficient for the transcriptional activation of the *fruB* promoter in the absence of F1P. However, the *fru* transcript increased significantly in the presence of both FruR and F1P in *in vitro* transcription. However, when HPr was added to this reaction mixture, the intensity of the *fruB* transcript peak decreased to that of the control sample. Thus, we confirmed that dephosphorylated HPr inhibits the FruR-mediated transcriptional activation of the *fru* operon, both *in vivo* and *in vitro*.

HPr does not affect the affinities of FruR for F1P or DNA

Transcriptional activation of the *fru* operon requires the FruR–F1P complex binding to the DNA operator *fruB* O1 (FruR-binding site 1), which is located between –35 and –10 elements of the *fru* promoter (18). Because the spacer length between the –35 and –10 elements in the *fru* promoter of *V. cholerae* is unusually long (20 bp), the structural modification of DNA upon binding of the FruR–F1P complex is essential for RNAP binding to the promoter (18,44). Therefore, we hypothesized dephosphorylated HPr might affect the FruR-mediated transcriptional activation of the *fru* operon in three possible ways: (i) by affecting the binding of an effector molecule to FruR, (ii) by affecting the binding affinity of FruR for the operator in the presence of F1P or (iii) by affecting the binding of RNAP to the promoter. To test the first possibility, we measured the binding affinity of FruR for F1P in the presence and absence of HPr using isothermal titration calorimetry (ITC) (Figure 3C). F1P was incrementally titrated into FruR alone or FruR saturated with an excess amount of HPr, and the binding heat signals generated per mol of injected F1P were plotted as a function of the molar ratio [F1P]/[FruR] (32). In the absence of HPr, F1P binding to FruR is exothermic; binding enthalpy (ΔH) is -80.0 ± 4.0 kcal/mol, the K_d value was 133 ± 0.51 μ M, and $-T\Delta S$ was 74.5. Interestingly, the binding enthalpy and binding affinity of F1P for FruR were not significantly changed in the presence of HPr ($\Delta H = -80.0 \pm 12.1$ kcal/mol, $K_d = 126 \pm 16.5$ μ M, $-T\Delta S = 74.6$) (Figure 3C). The possibility of binding of

F1P to HPr was ruled out using ITC (Supplementary Figure S2, left panel). Although F1P is the only metabolite effector of FruRs in *E. coli* and *Pseudomonas putida* (45–47), we examined the possibility of using fructose 1,6-bisphosphate (FBP) as an effector. However, ITC experiments showed FBP did not bind to FruR (Supplementary Figure S2, right panel). Therefore, these data exclude the possibility that HPr affects the specific binding of FruR to its effector molecule.

To test the second possibility, we performed an EMSA with the 338-bp probe covering the entire *fruR*–*fruB* intergenic region (18) and FruR in the absence and presence of F1P or HPr (Figure 3D). As we have recently shown (18), F1P weakens the binding affinity of FruR to the operator site, *fruB* O1 but does not release FruR from DNA. Interestingly, HPr supershifted the electrophoretic mobility of the FruR–DNA complexes (indicated with red arrows) but did not significantly affect the binding pattern of FruR for the operators, regardless of the presence of F1P. These data rule out the second possibility and show that FruR can still bind to the operator region, even when complexed with HPr. For transcriptional activation of the *fru* operon, only *fruB* O1 is required out of three FruR-binding sites in the *fruB* promoter (18). To further confirm that HPr does not significantly affect the binding affinity of FruR to *fruB* O1, EMSA was performed with the 338-bp probe containing intact *fruB* O1 and two mutated binding sites at *fruB* O2 and *fruB* O3 (O1 probe) in the presence of increasing concentrations of FruR, and the binding affinity of FruR for *fruB* O1 was measured in the presence or absence of F1P and HPr (18). In this study, the binding affinity of FruR for *fruB* O1 decreased 3-fold in the presence of F1P, as previously reported (18), regardless of the presence of HPr (Supplementary Figure S3A). Interestingly, regardless of the presence of F1P, HPr did not induce a significant change in the binding affinity of FruR for *fruB* O1 (Supplementary Figure S3B).

HPr inhibits the FruR/F1P-facilitated binding of RNAP to the *fru* promoter

To test the third possibility, we performed DNase I footprinting assays with a hybrid RNAP holoenzyme comprising the *E. coli* core enzyme, *V. cholerae* σ^{70} , FruR, and HPr, in the absence or presence of F1P, using a 6' FAM-labelled probe spanning from –199 to +339 relative to the TSS (18). As previously reported, FruR protected the DNA region from –27 to –12 and –5 to +11 relative to the TSS, which correspond to *fruB* O1 and *fruB* O2, respectively (marked with red boxes in Figure 4A) and, in the presence of F1P, the protection by FruR in the DNA region corresponding to *fruB* O1 was slightly decreased. When HPr was added to the DNase I reaction mixture with FruR, FruR protection was not affected in the DNA regions corresponding to *fruB* O1 and *fruB* O2, regardless of the presence of F1P (Figure 4A), which is consistent with the EMSA results (Figure 3D and Supplementary Figure S3). We have recently shown that the hybrid RNAP holoenzyme protects the DNA region from –76 to –7 from DNase I digestion (18). However, when RNAP was added to the DNase I reaction mixture with FruR, protection by the RNAP holoenzyme in the region encompassing –71 to –28, which contains a binding site

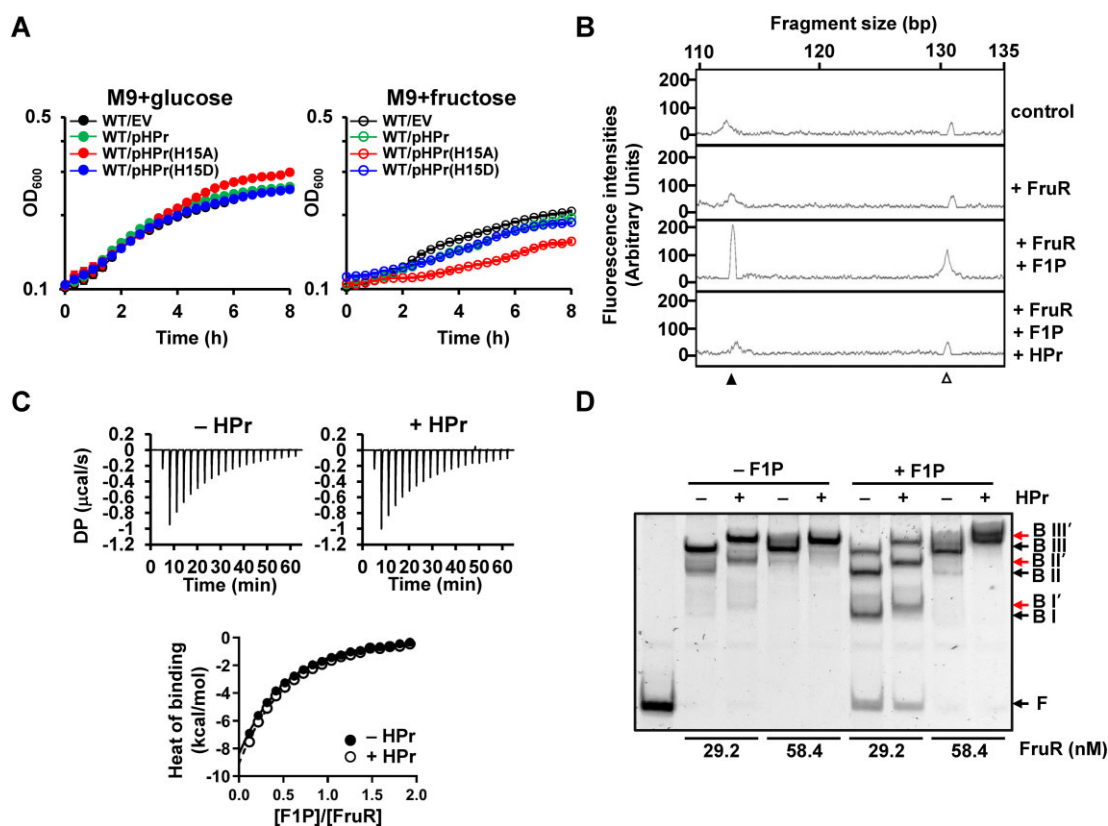


Figure 3. Effects of dephosphorylated HPr on FruR activity. (A) Comparison of the growth of the wild-type strains harbouring a plasmid expressing wild-type HPr or its mutant form (H15A or H15D) in M9 medium supplemented with indicated sugar. The means and standard deviations of three independent measurements are shown. EV, empty vector. (B) *in vitro* transcription assay was conducted to further confirm the HPr-mediated inhibition of FruR-dependent *fruB* transcription. The 418-bp template DNA spanning from -99 to +319 bp relative to the transcription start site (TSS) was incubated with *V. cholerae* RNAP holoenzyme (RpoA, RpoB, RpoC, RpoZ, and RpoD) in the absence or presence of FruR, F1P or HPr as indicated. The resulting RNA products were purified and annealed with HEX-labelled primer, which anneals to the region from +92 to +112 relative to the TSS and extended using reverse transcriptase. A 133-bp HEX-labelled DNA added to each reaction as a loading control is indicated by an open triangle, and the 112-bp *fruB* transcript is indicated by a closed triangle. Fragment sizes were determined by comparison to the internal molecular weight standards, and nucleotide positions relative to the TSS are indicated. (C) FruR-binding affinities for F1P in the presence or absence of HPr were determined using ITC. In ITC, 1 mM F1P is incrementally titrated into 0.1 mM FruR alone (upper panel, -HPr) or a mixture of 0.1 mM FruR and 0.2 mM HPr (upper panel, +HPr). The binding heat signals generated per mol of injected F1P are plotted as a function of molar ratio [F1P]/[FruR] (lower panel) (32). Curve fitting model is one set of binding. (D) Effect of HPr on FruR binding to the *fruB* promoter was assessed in the absence or presence of F1P by EMSA. The 338-bp probe covering the entire *fruR*-*fruB* intergenic region was incubated with FruR in the absence and presence of 0.5 mM F1P or 105.6 nM HPr and analysed on a 6% polyacrylamide gel.

of the C-terminal domains of the α -subunits of RNAP (48) was abolished (marked with red lines in Figure 4A) (18). Therefore, we demonstrated that FruR efficiently competes with RNAP for binding to the promoter, thus inhibiting transcriptional initiation in the absence of F1P (18). However, when F1P was added to the DNase I reaction mixture containing both RNAP and FruR, the RNAP holoenzyme-mediated protection of the regions encompassing -71 to -40 and -27 to -21 became stronger (blue lines in Figure 4A). Furthermore, the sequence corresponding to the TSS (marked with an asterisk in Figure 4A) became hypersensitive to DNase I, which implies that the FruR-F1P complex induces structural modifications in the *fru* promoter (18). However, interestingly, when HPr was added to this mixture, the protection of both regions encompassing -71 to -40 and -27 to -21 was abrogated (compare the regions marked in the blue lines in Figure 4A), and the signal at the TSS was almost completely abolished so the transcription of the *fru* operon cannot be initiated, which agrees with

the results of the *in vitro* transcription assay (Figure 3B). When HPr was added to the DNase I reaction mixture, with FruR and RNAP holoenzyme in the absence of F1P, the binding of RNAP to the promoter was completely abolished, as expected. Consequently, together with the above results, footprinting experiments implied that dephosphorylated HPr binds to FruR and interferes with FruR/F1P-facilitated RNAP binding to the *fru* promoter, preventing transcriptional initiation (Figure 4B).

Structural basis for FruR binding to dephosphorylated HPr

To investigate the precise mechanism of regulation of FruR-mediated transcriptional activation by HPr, we solved the crystal structure of the FruR-HPr complex from *V. cholerae* (VcFruR-VcHPr) at a resolution of 2.0 Å (Figure 5A and Supplementary Figure S4). In the crystal structure, the asymmetric unit contained a VcFruR dimer and two VcHPr proteins bound to each VcFruR monomer, forming a het-

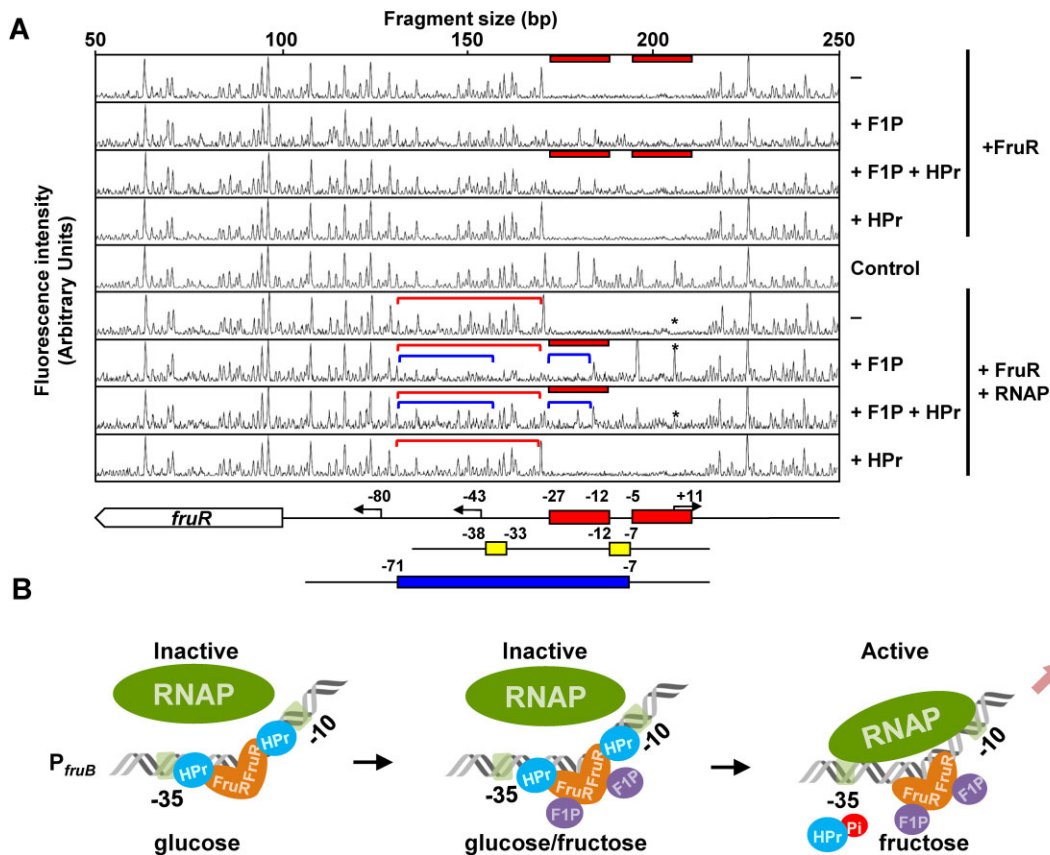


Figure 4. HPr inhibits the binding of RNAP to the *fru* promoter. (A) The effect of HPr on the FruR-mediated facilitation of RNA polymerase binding to the *fruB* promoter was assessed by the DNase I footprinting assay. A 6-FAM-labelled 538-bp *fruB* probe (200 ng; 30.6 nM) was incubated with FruR (0.45 μ M) in the presence of different combinations of F1P (2 mM), HPr (4.28 μ M), and hybrid RNAP holoenzyme (0.04 μ M *E. coli* core RNAP and 0.46 μ M *V. cholerae* σ^{70}) as indicated. The DNA regions protected from DNase I digestion by FruR (red bars) and RNAP (a blue bar) were then determined. The DNA regions encompassing -71 to -28 are indicated with red lines, and the DNA regions encompassing -71 to -40 and -27 to -21 relative to the TSS are indicated with blue lines. The TSS of the *fru* operon is marked with red asterisks. Schematic diagrams of the *fruR*–*fruB* intergenic region are shown below, and FruR-binding sites, -35 and -10 elements, and RNAP-binding sites are depicted in red, yellow, and blue bars, respectively. The bent arrows indicate the TSSs of the *fru* operon and *fruR* with nucleotide positions relative to the *fruB* TSS. The fluorescence intensity of the 6-FAM-labelled fragments is shown on the y-axis of each electropherogram, and fragment sizes were determined by comparison with the internal molecular weight standards. (B) Schematic view of the proposed mechanism of HPr-mediated inhibition of the transcriptional activation of the *fru* operon in *V. cholerae*.

erotetramer. The overall structure of the VcFruR dimer is like that of *E. coli* FruR (EcFruR) (PDB codes: 2IKS and 7DOB) (49) and *P. putida* FruR (PpFruR) (PDB codes: 3O74 and 3O75) (45,46) for 441 and 501 C α atoms with r.m.s.d. of 1.592 and 4.291 Å, respectively. The structure of VcFruR from the VcFruR–VcHPr complex was not significantly different from the modelled apo-VcFruR structure explored in our previous study (18). The electron density corresponding to the VcFruR DNA-binding domain (DBD; residues 1–59), which comprises the helix-turn-helix (HTH) motif and the hinge helix that connects to the effector binding domain, was not identified, possibly due to the spontaneous cleavage of DBD during crystallization (49). This speculation is supported by the lack of space for the DBD, considering the position of adjacent symmetry molecules in the crystal packing (Supplementary Figure S5).

In a previous study, we reported that the side chains of the conserved residues responsible for F1P binding in VcFruR could be similarly oriented with the corresponding residues in PpFruR (18). This assumption was verified by superim-

posing the structure of VcFruR onto that of the PpFruR–F1P complex (PDB code: 3O75) (45) and we clearly observed that the side chains of Asn73, Ser75, Tyr76, Asp148, Arg149, Arg197, Ser246 and Arg320 of VcFruR are identically oriented with the corresponding residues of PpFruR (Supplementary Figure S6). It is also worth noting that the F1P binding cavity is apart from the interaction interface between VcFruR and VcHPr (Figure 5A and Supplementary Figure S6). Therefore, it is highly likely that the binding of VcFruR with F1P and VcHPr does not affect each other, which is consistent with the results of the EMSA and footprinting assays (Figures 3D and 4A, Supplementary Figure S3).

A common face on HPr interacts with all its partner proteins in *E. coli* (50). In particular, several amino acid residues in α -helix 1 (α 1) and α -helix 2 (α 2) of *E. coli* HPr (EcHPr) are responsible for direct interaction with Rsd, LsrK and MtlR (7,51–52). Because these amino acids are well conserved in VcHPr (Supplementary Figure S7), we hypothesized that the mode of interaction between EcHPr and its partners could also be applied to the interaction between

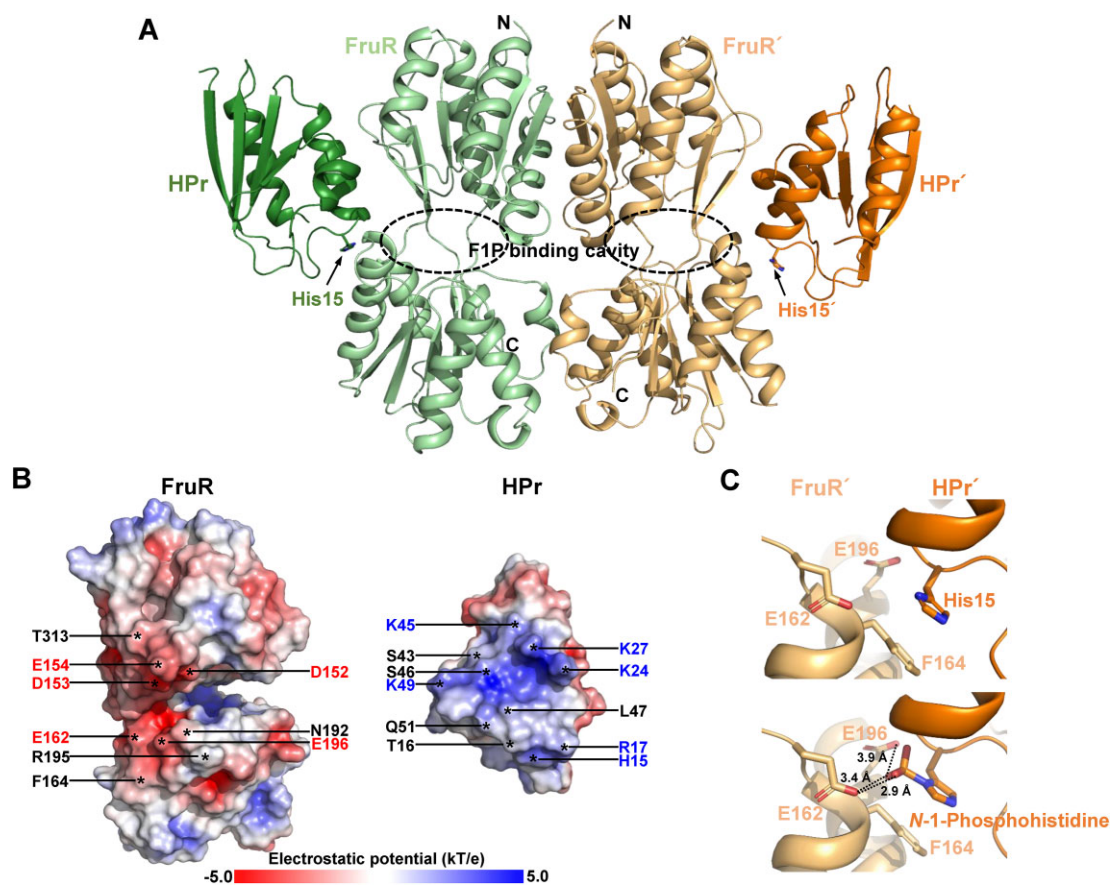


Figure 5. Overall structure of the FruR–HPr complex. (A) Ribbon diagram of the *V. cholerae* FruR–HPr complex (VcFruR–VcHPr). The VcFruR–VcHPr complex is a heterotetramer composed of one VcFruR dimer and two VcHPr monomers. The asymmetric unit contains one VcFruR–VcHPr heterotetramer, and VcHPr is independently bound to each VcFruR molecule. Each VcFruR monomer in the VcFruR dimer is coloured light green and light orange, whereas the bound VcHPr molecule for each VcFruR is shown as dark green and dark orange, respectively. His15 residues from two VcHPr are shown as sticks, and the F1P binding cavity is denoted with a dotted black ellipse. (B) Surface electrostatic potential of VcFruR and VcHPr. The Adaptive Poisson-Boltzmann Solver (APBS) was used to calculate the electrostatic potential at pH 7. The potential ranging from -5 kT/e to 5 kT/e is coloured as indicated by the coloured spectrum bar at the bottom. The potential lower than -5 kT/e is coloured in red, and that higher than 5 kT/e is coloured in blue. Amino acids located in the VcFruR–VcHPr interaction interface are indicated with asterisks. The acidic amino acids on the surface of VcFruR and the basic amino acids on the surface of VcHPr are labelled red and blue, respectively. (C) Residues from VcFruR near His15 of VcHPr are shown as sticks and labelled. Dephosphorylated His15 interacts with Phe164 through π – π stacking and is located close to Glu162 and Glu196 of VcFruR (upper panel). A modelled structure that replaces His15 of VcHPr with *N*-1-phosphohistidine shows that the distances between the phosphate group of *N*-1-phosphohistidine from VcHPr and carboxyl oxygen atoms in Glu162 and Glu196 of VcFruR are within 4 Å (lower panel). The oxygen, nitrogen and phosphorus atoms are coloured in red, blue and orange, respectively.

VcHPr and VcFruR. Dephosphorylated EcHPr binds directly to Rsd, LsrK and MtlR, which possess three common structural features for HPr binding (7). First, a hydrophobic pocket can recognize Phe48 of HPr. Second, several acidic residues can bind to basic amino acids on the surface of HPr. Third, one or two acidic residues are positioned close to His15 of HPr, and the binding of phosphorylated HPr, which forms *N*-1-phosphohistidine at the His15 position, cannot be established due to charge repulsion.

We examined whether these structural features were also present in the VcFruR–VcHPr complex structure. First, Phe48 of VcHPr was forwarded to the F1P binding cavity of VcFruR and positioned near the shallow groove, which is surrounded by hydrophobic residues at the interface between VcFruR and VcHPr (Supplementary Figure S8). Second, the electrostatic surface potential showed that acidic amino acids such as Asp152, Asp153, Glu154, Glu162 and

Glu196 from VcFruR were clustered in the interaction interface and closely encountered the basic amino acids of VcHPr, including His15, Arg17, Lys24, Lys27, Lys45 and Lys49 (Figure 5B). However, there was no direct interaction between the acidic amino acid of VcFruR and the basic amino acid of VcHPr in our current structure. Third, we found that His15 of VcHPr was located close to two acidic amino acids, Glu162 and Glu196, of VcFruR. Furthermore, the imidazole ring of His15 of VcHPr forms a π – π stacking interaction with the phenyl ring of Phe164 from VcFruR (Figure 5C, upper panel). When His15 of VcHPr was modelled to be substituted with *N*-1-phosphohistidine (7,51), the distances between the phosphate group of *N*-1-phosphohistidine and Glu162/Glu196 of VcFruR were <4 Å, which is close enough to cause charge repulsion (Figure 5C, lower panel) and allows VcFruR to accommodate only the dephosphorylated VcHPr.

Polar interaction is crucial for FruR–HPr binding in *V. cholerae*

As mentioned in the previous section, the interaction interface between VcFruR and VcHPr was primarily formed by polar interactions. Two VcFruR–VcHPr interfaces of the heterotetramer (VcHPr–VcFruR::VcFruR'–VcHPr', where prime denotes the other molecule in the asymmetric unit) share almost identical polar interactions (Figure 6A). Detailed common interaction pairs are as follows in the order of VcFruR followed by VcHPr: the side-chain carboxyl group of Asp152 and the side-chain hydroxyl group of Ser46; the side-chain carboxyl group of Asp153 and the backbone amide nitrogen of Leu47/Phe48; the side-chain carboxyl group of Glu154 and the side-chain hydroxyl group of Ser43; the side-chain guanidinium group of Arg195 and the back-bone carbonyl oxygen of Gln51; the side-chain carboxyl group of Glu196 and the side-chain oxygen atom/the backbone amide nitrogen of Thr16; the side-chain oxygen atom or the backbone carbonyl oxygen of Thr313 and the side-chain amine group of Lys27. In addition, Glu162 of VcFruR forms a water-mediated polar interaction with His15 of VcHPr. The polar interactions between the backbone carbonyl oxygen of Asp153 (VcFruR) and the side-chain amine group of Lys27 (VcHPr), the side-chain carboxyl group of Glu196 (VcFruR) and the side-chain amine group of Gln51 (VcHPr) were found in only one interaction interface (Figure 6B, grey lines).

As both *Vibrionaceae* and *Enterobacteriaceae* belong to the Gammaproteobacteria class, the PTS components of *Vibrio* species have high amino acid sequence similarities with their *E. coli* orthologs (19). However, despite this similarity, several protein-protein interactions of PTS proteins reported in *Vibrio* species have not been observed in *E. coli* (7,12,19). In a previous study, we demonstrated that VcFruR is a homodimer and structurally distinct from other GalR–LacI family transcription factors, including EcFruR, which form a homotetramer (18). However, structural comparison and alignment of the amino acid sequence between VcFruR and EcFruR showed high structural similarity between the dimeric EcFruR and dimeric VcFruR (Supplementary Figures S9A and S9C). Furthermore, VcHPr showed 76.2% amino acid sequence identity with EcHPr (64 of 84 identical; Supplementary Figure S7). Interestingly, native PAGE revealed that there was no interaction between EcFruR and EcHPr (Supplementary Figure S9B). To understand the reason for the difference in the binding of FruR to HPr from *V. cholerae* and *E. coli*, we compared the amino acid residues of VcFruR crucial for the FruR–HPr interaction with those in EcFruR. EcFruR and VcFruR share the same amino acids at positions 152 and 154 but possess different amino acids at positions 153, 164, 195, 196 and 313 (Supplementary Figure S9C). To determine which amino acid are required as determinants for the specific interaction with HPr, we substituted the amino acids at positions 153, 164, 196 and 313 of VcFruR individually with those found in EcFruR (marked with arrows), and the interaction between each and WT VcHPr was examined by native PAGE. Although the T313P and F164Q mutants could still interact with VcHPr, the D153R, and E196L mutants were not (Figure 6C), supporting that po-

lar interactions involving positions 153 and 196 are crucial for FruR–HPr interaction in *V. cholerae*.

Glucose preference over fructose is accomplished by HPr-mediated inhibition of FruR activity

According to a previous study, the interaction between dephosphorylated HPr and MtlR in *E. coli* determines the preference between glucose and mannitol (6). Therefore, we assumed that if the HPr-mediated inhibition of FruR was released, the preference between glucose and fructose would disappear in *V. cholerae*. In order to test this hypothesis, we sought to find a mutant form of HPr that still retains phosphotransferase activity but does not interact with FruR. Based on the information in Figure 6 and Supplementary Figure S7, we made mutations on Thr16, Lys27 and Ser46 to Ala, Glu and Asp, respectively. The T16A mutant still interacted with FruR, however, K27E and S46D mutants did not (Supplementary Figure S10). To determine whether the HPr mutants retained their phosphotransferase activity, we compared the growth of the $\Delta ptsH$ strains carrying expression vectors for each HPr mutant, wild-type HPr or an empty vector. The $\Delta ptsH$ strain carrying pHPr(T16A) showed growth similar to the strain with an empty vector, while the growth rates of $\Delta ptsH$ strains carrying pHPr(S46D) or pHPr(K27E) were similar to the $\Delta ptsH$ strain carrying pHPr(WT), suggesting that these mutants still have phosphotransferase activity (Supplementary Figure S10B). Next, we compared the growth, sugar consumption, and *fruB* expression in $\Delta ptsH$ strains carrying an empty vector, pHPr(WT), or pHPr(S46D) on glucose and fructose (Figure 7). The strain carrying an empty vector showed slower growth and consumed glucose and fructose simultaneously (Figure 7A, upper panel). While the strain carrying pHPr(WT) preferred glucose over fructose (Figure 7B, upper panel), the strain carrying pHPr(S46D) consumed both sugars simultaneously and grew faster than the strain carrying pHPr(WT) (Figure 7C, upper panel). As expected, the *fruB* expression was repressed during glucose utilization in the strain carrying pHPr(WT) (Figure 7B, lower panel), while elevated *fruB* expression was observed throughout the incubation period in both the strains carrying an empty vector and a pHPr(S46D) (Figure 7A and C, lower panels). These data suggest that the interaction between HPr and FruR determines the preference between glucose and fructose in *V. cholerae*, just as the interaction between HPr and MtlR in *E. coli* determines the preference between glucose and mannitol (6).

The FruR–HPr complex structure is distinct from the CcpA–HPr complex structure

Protein–protein interactions can induce structural alterations and regulate the DNA-binding capacity of transcription factors (53). To investigate the structural changes in VcFruR upon binding of VcHPr or F1P and the consequent impact of structural changes in VcFruR on FruR-mediated transcription regulation in the presence or absence of fructose, we tried to solve the crystal structures of the full-length apo-VcFruR and VcFruR–F1P complex;

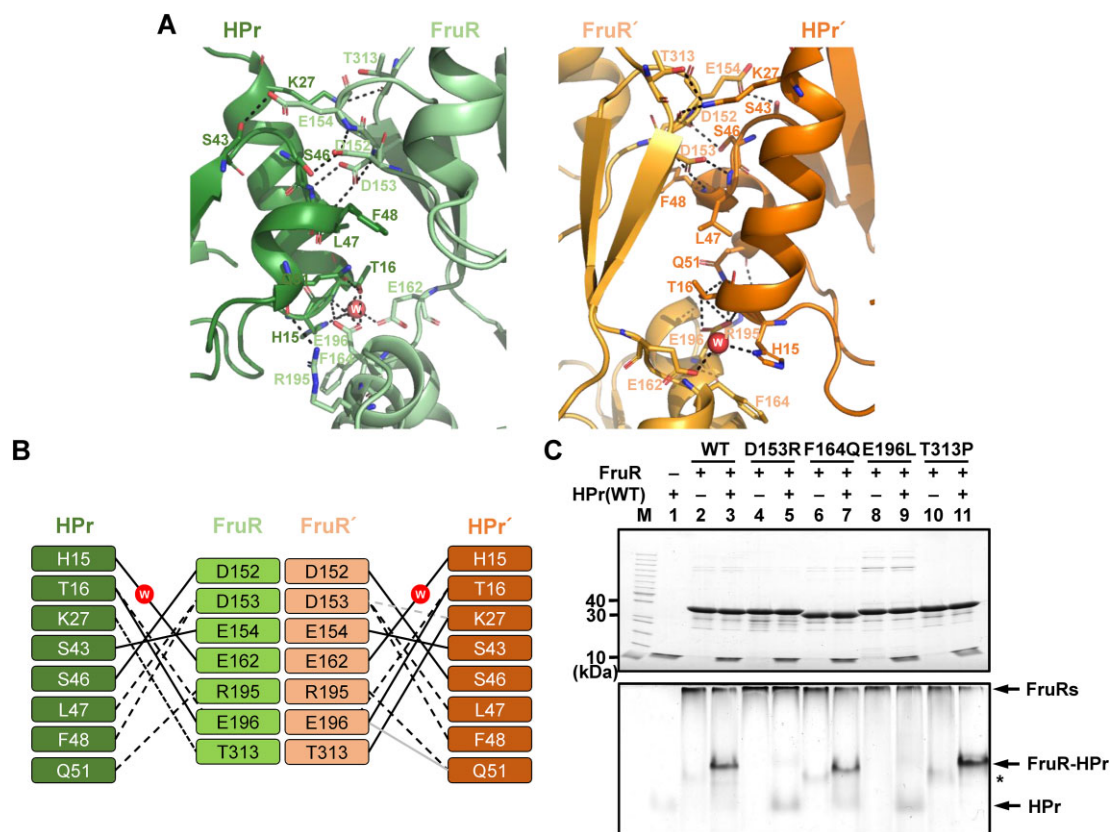


Figure 6. The polar interaction is crucial for the FruR–HPr binding. (A) Close-up views of two VcFruR–VcHPr interaction interfaces. The VcFruR and VcHPr molecules are shown as ribbon diagrams. The amino acids involved in the polar interactions between VcFruR and VcHPr are shown as sticks and labelled with the same colour as the protein molecule from which the labelled amino acids originated. Polar interactions found in the interaction interface are denoted as black dotted lines. One water molecule which mediates the polar interaction between His15 of VcHPr and Glu162 of VcFruR is shown as a red sphere. The oxygen and nitrogen atoms are coloured in red and blue, respectively. The overall colour schemes are the same as in Figure 5. (B) Schematic diagram denoting the amino acid interactions between VcFruR and VcHPr. Black lines indicate the amino acid pairs in which the interatomic distance is <5 Å. Solid lines denote the interaction between atoms in the side-chain of each VcFruR and VcHPr, whereas dotted lines indicate the interaction between atoms from the side-chain of VcFruR or VcHPr and from the backbone of the counterpart. The grey lines indicate the interaction between VcFruR and VcHPr, which is present only in one of two interaction interfaces. Red circles indicate the water molecule that mediates the polar interaction between E162 of VcFruR and H15 of VcHPr. (C) To examine the effect of polar interactions between HPr and FruR, amino acids at positions 153, 164, 195 and 313 of VcFruR were individually mutated to those of EcFruR, and these VcFruR mutants were incubated with or without wild-type HPr in buffer P and subjected to native PAGE in comparison with wild-type VcFruR. An asterisk indicates the bands of impurity protein in FruRs.

however, these efforts were unsuccessful. Because our current VcFruR–VcHPr complex structure lacks its DBD (Figure 5A), we compared the VcFruR–VcHPr complex with other GalR–LacI family transcriptional regulators whose function is regulated by the binding of HPr and has a similar structure and function like FruR.

The GalR–LacI family transcription factors are important in the coordination of catabolic, anabolic, and transport operons and are widely conserved in prokaryotes (54). However, the interaction between members of the GalR–LacI family and HPr has not been documented in Gram-negative bacteria, including *V. cholerae*. On the other hand, the carbon catabolite protein A (CcpA) has been shown to be regulated by HPr in two Gram-positive bacteria, *B. subtilis* (55) and *Priestia megaterium* (36). *Bacillus subtilis* CcpA (BsCcpA) directly binds to the promoters of various metabolic genes and plays a central role in CCR (3–4,36,55). In Gram-positive bacteria, besides PEP-dependent phosphorylation at His15, phosphorylation of HPr occurs at Ser46 through ATP-dependent enzymatic

phosphorylation by HPr kinase/phosphorylase (HPrK/P) (56). The bifunctional HPrK/P phosphorylates or dephosphorylates Ser46 of HPr by recognizing intracellular levels of FBP (9). Phosphorylation at Ser46 increases the affinity of HPr to CcpA (36,55,57) and the resulting HPr(Ser46-P)–CcpA complex stimulates the binding of CcpA to its target DNA sites called catabolite responsive elements (*cre*s) (57,58).

VcFruR and BsCcpA share a 20.5% amino acid sequence identity (Supplementary Figure S11A). In particular, the N-terminal HTH motifs of VcFruR and BsCcpA show a higher sequence identity of 32.1% than the overall sequence identity. The N-terminal DBD, including HTH, is a well-known structural characteristic of transcription factors from the GalR–LacI family (54,59). Furthermore, VcHPr and *B. subtilis* HPr (BsHPr) show a sequence identity of 38.3%, and His15 and Ser46 are well conserved in both proteins (Supplementary Figure S11B). Unlike *B. subtilis*, HPrK/P is not present in *V. cholerae*; therefore, the Ser46 residue of VcHPr cannot be phosphorylated.

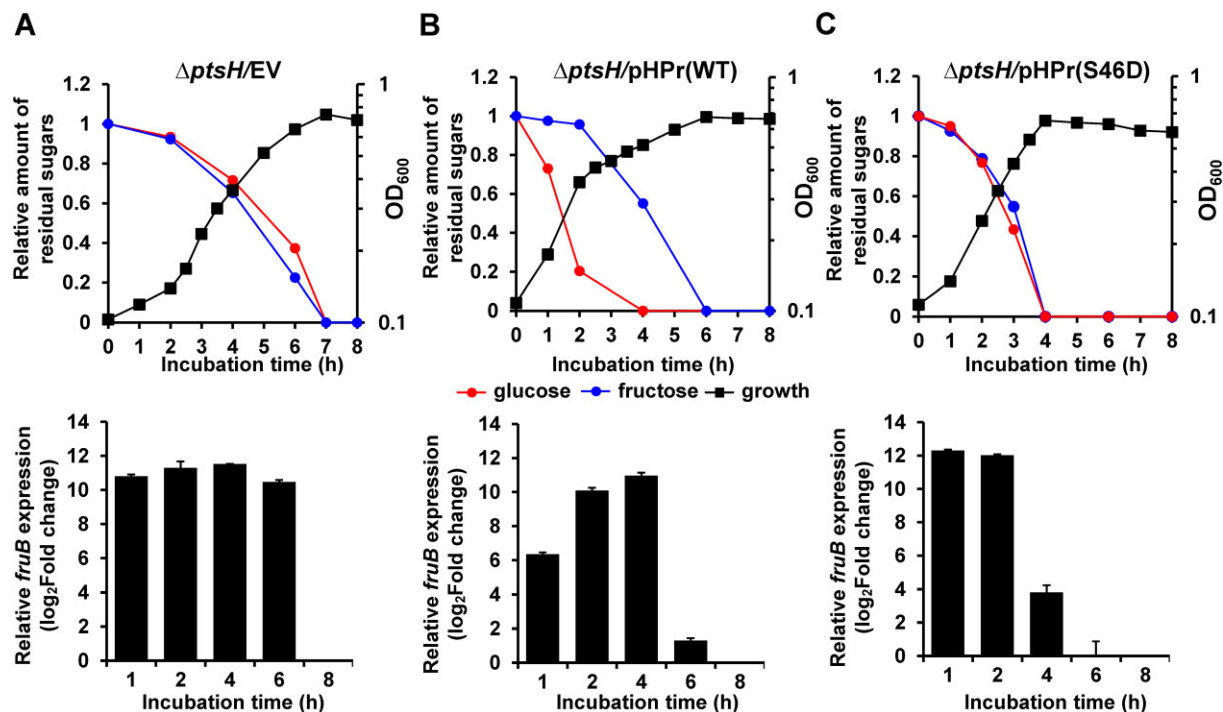


Figure 7. Glucose preference over fructose is accomplished by HPr-mediated inhibition of FruR activity. The upper panel shows the growth curves and remaining sugar concentrations in the medium, while the lower panel displays the relative transcript levels of *fruB*. These data were obtained during the growth of $\Delta ptsH$ strains harbouring an empty vector (A), an expression vector for wild-type HPr (B), or an HPr(S46D) expression vector (C) on glucose and fructose, at the indicated incubation times. The relative transcript levels of *fruB* in the strains harvested at the indicated incubation times were quantified by qRT-PCR. The mRNA levels are shown as relative values (\log_2 scale) to the cells harvested at the 8 h incubation time. The mean and standard deviation of three independent measurements are shown.

To explore the mode of HPr binding to FruR or CcpA and the effect of HPr phosphorylation at Ser46 on its binding to partner proteins, we compared the BsCcpA–BsHPr structure (PDB code: 3OQM) (55) with the VcFruR–VcHPr structure (Figure 8A). The overall structure and secondary structure topology of the regulatory domain are similar between VcFruR and BsCcpA for 414 C α atoms with an r.m.s.d. of 2.962 Å. At the interface of the BsCcpA–BsHPr interaction, residues located in $\alpha 1$, $\alpha 2$, and the turn between $\beta 1$ and $\alpha 1$ of BsHPr are implicated in the interaction with the surface exposed regions of BsCcpA αI and αIX (36). The conserved hydrophobic residues in αI and αIX of BsCcpA tightly interact with Ile47, Met48 and Met51 of BsHPr. Furthermore, Arg304 and Lys308 in αIX of BsCcpA interact directly with Ser46-P of BsHPr, whereas Tyr89 contributed to the maintenance of these specific interactions (Figure 8B) (36,55). Therefore, phosphorylation of Ser46 in BsHPr is essential to increase both binding specificity and the affinity for BsCcpA.

Unexpectedly, the interaction interface between VcFruR and VcHPr is formed at a position different from that of BsCcpA–BsHPr. Amino acids in the loop linking βD and βE (Asp152, Asp153 and Glu154), in the loop linking αIX and βK (Thr313), in the loop linking βE and αIV (Glu162), αIV (Phe164) and αV (Arg195 and Glu196) of VcFruR interact with amino acids in the loop linking $\beta 1$ and $\alpha 1$ (His15), $\alpha 1$ (Thr16 and Lys27), $\alpha 2$ (Leu47, Phe48 and Glu51), and in the loop linking $\alpha 2$ and $\beta 3$ (Ser43 and Ser46) of VcHPr (Figure 8A). The dephosphorylated

Ser46 of VcHPr makes polar interactions with Asp152 of VcFruR at a distance of 2.8 Å and is also closely located from Asp153 of VcFruR at a distance of 4.3 Å (Figure 8B). Therefore, we can safely assume that intrinsically dephosphorylated Ser46 of VcHPr is necessary to bind to VcFruR because phosphorylation of Ser46 can cause charge repulsion and steric hindrance between Ser46 of VcHPr and Asp152/Asp153 of VcFruR (Figure 8B) (52). When Ser46 of VcHPr was substituted with aspartate to mimic Ser46-P of VcHPr, VcFruR did not interact with VcHPr (Supplementary Figure S10A).

DISCUSSION

Here, we show that dephosphorylated HPr directly binds to FruR and inhibits transcriptional activation of the *fru* operon mediated by the FruR–F1P complex in *V. cholerae* (Figure 4). VcHPr did not affect the DNA-binding affinity of VcFruR, regardless of the presence of F1P (Figures 3D, 4A, and Supplementary Figure S3), but prevented the FruR-mediated facilitation of RNAP binding to the promoter in the presence of F1P (Figure 4A). The K_d value for VcFruR to F1P is approximately 120 μM (Figure 3B), which is slightly lower than the intracellular concentration of F1P in bacterial cells grown on fructose ($\sim 150 \mu M$) (60). Therefore, we assume that VcHPr's regulation of transcription of the *fru* operon plays an important role in inhibiting the unnecessary expression of PTS^{Fru} when *V. cholerae* cells are exposed to an environment where a preferred carbon

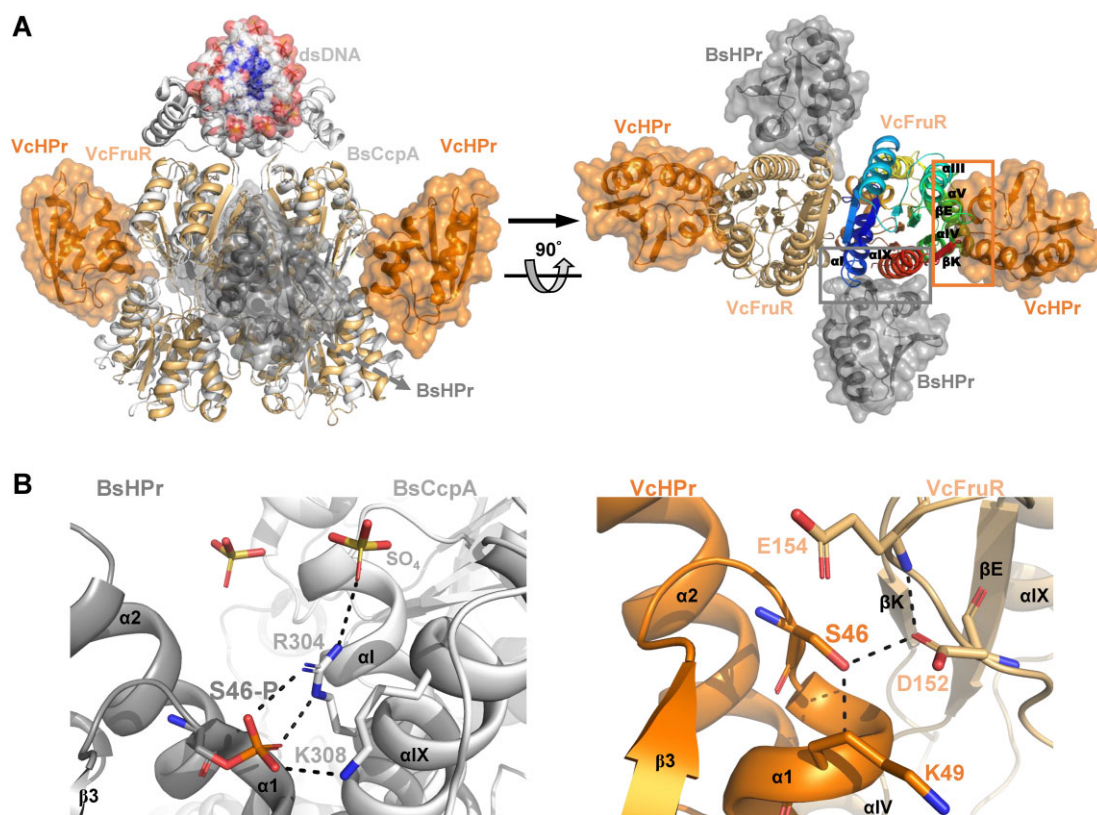


Figure 8. The FruR–HPr complex structure is distinct from that of the CcpA–HPr complex structure. (A) Ribbon diagrams show two orthogonal views of the VcFruR–VcHPr complex structure superimposed onto the BsCcpA–BsHPr(Ser46-P)–DNA complex structure. To distinguish each protein molecule, VcFruR (light orange), VcHPr (dark orange), BsCcpA (light grey) and BsHPr (dark grey) are coloured distinctly. VcHPr, BsHPr and a 16-bp double-stranded DNA bound to BsCcpA (shown as sticks, oxygen atoms in red and nitrogen atoms in blue) are veiled by transparent surfaces. Each protein is labelled with the same colour as the ribbon diagram. On the right, BsCcpA and its bound DNA molecules are omitted, and one VcFruR molecule is coloured progressively from blue at the N-terminus to red at the C-terminus to show the different modes of interactions between VcFruR–VcHPr and BsCcpA–BsHPr. The interaction interfaces of VcFruR–VcHPr and BsCcpA–BsHPr are denoted as orange and grey rectangles, respectively, and the secondary structure elements of VcFruR (\approx BsCcpA) implicated in the interaction interface are labelled. (B) Close-up views of the local environment around Ser46-P from the BsCcpA–BsHPr(Ser46-P)–DNA complex (left panel) and Ser46 from the VcFruR–VcHPr complex (right panel). The phosphate group of Ser46-P of BsHPr (dark grey) has polar interactions with Arg304 and Lys308 of BsCcpA (light grey). On the other hand, the unphosphorylated Ser46 of VcHPr (dark orange) interacts directly with Asp152 of VcFruR (light orange). All amino acids involved in the polar interaction between Ser46 of HPr and residues from FruR/CcpA are shown as sticks along with two sulphate ions in the BsCcpA–BsHPr(Ser46-P)–DNA complex structure. The oxygen, nitrogen, sulphur, and phosphorus atoms are coloured in red, blue, yellow and orange, respectively.

source, such as glucose, is available besides fructose (Figure 1).

The EI of the PTS sequentially transfers a phosphate group from PEP to HPr, EIIA and EIIB. If the corresponding PTS substrate is present, EIIB transfers this phosphoryl group to the carbohydrate during its transport through EIIC, leading to a decrease in the phosphorylated state of the corresponding PTS components (1). The PTS^{Fru} comprises FruB and FruA (Figure 2D) and has its own HPr-like domain, FPr, fused to an EIIA domain in FruB, which transfers the phosphate group from EI to the fructose molecule transported through FruA (EIIB'BC). HPr participates in a PEP-dependent phosphotransfer reaction during fructose transport in a strain lacking FPr (14,18,42). Therefore, a *V. cholerae* strain lacking both HPr and FPr exhibits severe growth defects on fructose (11). We observed that more than half of HPr was phosphorylated in *V. cholerae* cells grown on fructose (Figure 2D), suggesting that the main route of fructose transport may employ the PTS phosphorylation cascade through FruB rather than through HPr

in a WT strain. In particular, the HPr phosphorylation level in the presence of fructose in *V. cholerae* is similar to that in the presence of mannitol in *E. coli*, where the phosphorylation state of HPr determines the preference for glucose over mannitol (6,7).

The small intestine is the main organ for dietary fructose clearance (61), in which approximately 20 mM fructose is present (62). According to a recent study, when *V. cholerae* infects the host, the expression of the genes coding for the PTS^{Fru} components increases in response to intestinal fructose, which contributes to the increase in toxin expression and intestinal colonization of *V. cholerae* (24). Therefore, elucidation of the transcriptional regulation of the *fru* operon is crucial for studying the carbon source-driven alteration of pathogenicity in *Vibrio* species (63).

Structural analysis of the VcFruR–VcHPr complex showed that the binding mode of the two proteins is similar to that of HPr with MtlR, Rsd and LsrK in *E. coli* (6–7,52). The three common features found in HPr partner proteins are (i) the presence of a hydrophobic region that recognizes

Phe48 of HPr (Supplementary Figure S8), (ii) a cluster of charged amino acids that can make polar interactions with the oppositely charged amino acids in HPr (Figure 5B) and (iii) one or two acidic amino acids near His15 from HPr (Figure 5C). Regarding the second feature, electrostatic interactions have been demonstrated to be important for the interactions between EcHPr and partner proteins (7). Although no direct electrostatic interactions were observed between amino acids with different charges at the interaction interface between VcFruR and VcHPr, we found extensive polar interactions between VcFruR and VcHPr (Figures 6A and B). Therefore, we hypothesized that common features in the mode of HPr binding to partner proteins in *E. coli* can be applied to HPr-involved protein-protein interactions in *V. cholerae*. Several amino acids of VcFruR involved in the polar interaction with VcHPr are not conserved in EcFruR (Supplementary Figure S9C), and substituting these residues into the corresponding sequences of EcFruR caused the failure to interact with VcHPr (Figure 6C).

Because the structure of VcFruR in our current VcFruR–VcHPr complex lacks a DBD (Figure 5A) (49), it was not possible to directly demonstrate how HPr regulates FruR-mediated transcriptional activation of the *fru* promoter. It is likely that the binding of VcHPr does not induce notable structural changes in the overall structure of VcFruR, since VcHPr does not affect the affinity of VcFruR for F1P (Figure 3C) and the local F1P binding environment of VcFruR in its complex with VcHPr is almost similar to that of the PpFruR–F1P complex (Supplementary Figure S6). Taken together with the *in vitro* data showing that VcHPr does not affect the DNA binding of VcFruR (Figure 3D and Supplementary Figure S3), the structure of the VcFruR–VcHPr complex provides evidence that HPr binding to FruR can occur independently of DNA or F1P. In our previous study, we suggested that the transcriptional regulatory mechanism of VcFruR might be similar to that of *E. coli* MerR (18). In *E. coli*, MerR-type transcription factors CueR and EcmrR interact with non-conserved regions of the σ^{70} factor (σ_{NCR}), which contribute to the transcription activation by providing auxiliary roles in interaction between RNAP and DNA (64,65). Therefore, it can be assumed that HPr blocks the interaction between FruR and σ^{70} of the RNAP holoenzyme. Interestingly, the structural superimposition of the VcFruR–VcHPr–*fruB*O1 DNA complex model onto the *E. coli* CueR–TAC (transcription activation complex) (66), with Ec σ^{70} replaced by the AlphaFold 2 model of the full-length Vc σ^{70} , revealed that the so-called disordered acidic loop in the σ_{NCR} is close to the negatively charged surface of one HPr protomer within a distance of 15 Å (Supplementary Figure S12). This close proximity may lead to charge repulsion, hindering the interaction between the σ_{NCR} of Vc σ^{70} and VcFruR. Therefore, we propose that the charge repulsion between HPr and σ^{70} may prevent the interaction between the RNAP holoenzyme and VcFruR, thus inhibiting the VcFruR–F1P complex-mediated facilitation of RNAP binding to the promoter (Figure 4B).

This is the first study to examine the interaction between FruR and HPr and there has been no crystal structure of the protein complex between the GalR–LacI family of transcription factors and HPr has been determined, with the

exception of the CcpA–HPr complexes (36,55). In *B. subtilis*, HPr regulates the DNA-binding affinity of transcriptional regulator CcpA through direct binding (57,58). Thus, we compared the structure of the BsCcpA–BsHPr complex with that of the VcFruR–VcHPr complex (Figure 8A). Despite the high structural similarities between BsCcpA and VcFruR and between BsHPr and VcHPr (Supplementary Figure S11), the HPr binding interfaces are established in different positions in VcFruR and BsCcpA, and the mode of HPr binding to each transcription regulator is also different (Figure 8). Thus, we assume that the inhibition of VcFruR-mediated transcriptional activation of the *fru* promoter by VcHPr is not established by directly regulating the DNA-binding affinity of VcFruR or VcFruR–F1P, unlike BsHPr, which affects the DNA-binding affinity of BsCcpA.

The cAMP–CRP complex is known to play an important role in the glucose-mediated CCR mechanism in many bacteria (1,3–5). However, in *Salmonella enterica* Typhimurium, glucose-mediated catabolite repression of the PTS^{Fru} genes occurs independently of CRP and cAMP (42). Recently, it was reported that the CRP–cAMP complex may act as a transcriptional activator of the *fru* operon in *V. cholerae* (40). However, this is not supported by the results of a chromatin immunoprecipitation-sequencing (ChIP-seq) study, which showed that CRP does not bind to the *fru* promoter *in vivo* in fructose-grown *V. cholerae* cells (67). This suggests that the CRP–cAMP complex has limited effect on the transcription of the *fru* operon. Thus, we propose that the glucose-mediated transcriptional regulation of the *fru* operon in *V. cholerae* is primarily mediated by the interaction between FruR and HPr. In conclusion, the molecular mechanism by which HPr regulates the FruR-mediated facilitation of RNAP binding to the *fru* promoter presents a new perspective on the PTS-dependent regulation of transcriptional factors that coordinate the transcription of carbon catabolic genes (5).

DATA AVAILABILITY

The atomic coordinates and structure factors of FruR–HPr complex (PDB code: 7X7H) have been deposited in the Protein Data Bank (www.rcsb.org). The datasets used and/or analyzed during the current study are available from the corresponding author on reasonable request.

SUPPLEMENTARY DATA

Supplementary Data are available at NAR Online.

ACKNOWLEDGEMENTS

The authors thank the beamline scientists at beamlines 5C, 7A and 11C of the Pohang Light Source for their support for X-ray diffraction data collection. The authors also thank Jaejun Choi (Seoul National University) for assistance in ITC experiment, Dr Young-Ha Park, Dr Hey-Min Kim and Dr Kyoo Heo for helpful discussions.

FUNDING

National Research Foundation (NRF) of Korea [NRF-2018R1A5A1025077, NRF-2019R1A2C2004143 to C.-K.

Y., S.-H. L., Y.-J.S.; NRF-2021R1A6A3A01086821 to C.-K.Y.; RS-2022-00164721, NRF-2020R1F1A1057780 to M.-K.K.]; Ministry of Science and ICT (MSIT) [The internal R&D program of KAERI(523210) to J.Z. and M.-K.K.]. Funding for open access charge: National Research Foundation of Korea [NRF-2019R1A2C2004143].
Conflict of interest statement. None declared.

REFERENCES

- Deutscher, J., Francke, C. and Postma, P.W. (2006) How phosphotransferase system-related protein phosphorylation regulates carbohydrate metabolism in bacteria. *Microbiol. Mol. Biol. Rev.*, **70**, 939–1031.
- Deutscher, J., Aké, F.M., Derkaoui, M., Zébré, A.C., Cao, T.N., Bouraoui, H., Kentache, T., Mokhtari, A., Milohanic, E. and Joyet, P. (2014) The bacterial phosphoenolpyruvate:carbohydrate phosphotransferase system: regulation by protein phosphorylation and phosphorylation-dependent protein-protein interactions. *Microbiol. Mol. Biol. Rev.*, **78**, 231–256.
- Görke, B. and Stülke, J. (2008) Carbon catabolite repression in bacteria: many ways to make the most out of nutrients. *Nat. Rev. Microbiol.*, **6**, 613–624.
- Deutscher, J. (2008) The mechanisms of carbon catabolite repression in bacteria. *Curr. Opin. Microbiol.*, **11**, 87–93.
- Galinier, A. and Deutscher, J. (2017) Sophisticated regulation of transcriptional factors by the bacterial phosphoenolpyruvate: sugar phosphotransferase system. *J. Mol. Biol.*, **429**, 773–789.
- Choe, M., Park, Y.H., Lee, C.R., Kim, Y.R. and Seok, Y.J. (2017) The general PTS component HPr determines the preference for glucose over mannitol. *Sci. Rep.*, **7**, 43431.
- Choe, M., Min, H., Park, Y.H., Kim, Y.R., Woo, J.S. and Seok, Y.J. (2019) Structural insight into glucose repression of the mannitol operon. *Sci. Rep.*, **9**, 13930.
- Park, Y.H., Lee, B.R., Seok, Y.J. and Peterkofsky, A. (2006) *In vitro* reconstitution of catabolite repression in *Escherichia coli*. *J. Biol. Chem.*, **281**, 6448–6454.
- Deutscher, J., Küster, E., Bergstedt, U., Charrier, V. and Hillen, W. (1995) Protein kinase-dependent HPr/CcpA interaction links glycolytic activity to carbon catabolite repression in gram-positive bacteria. *Mol. Microbiol.*, **15**, 1049–1053.
- Warner, J.B. and Lolkema, J.S. (2003) CcpA-dependent carbon catabolite repression in bacteria. *Microbiol. Mol. Biol. Rev.*, **67**, 475–490.
- Houot, L., Chang, S., Absalon, C. and Watnick, P.I. (2010) *Vibrio cholerae* phosphoenolpyruvate phosphotransferase system control of carbohydrate transport, biofilm formation, and colonization of the germfree mouse intestine. *Infect. Immun.*, **78**, 1482–1494.
- Kim, H.M., Park, Y.H., Yoon, C.K. and Seok, Y.J. (2015) Histidine phosphocarrier protein regulates pyruvate kinase A activity in response to glucose in *Vibrio vulnificus*. *Mol. Microbiol.*, **96**, 293–305.
- Park, S., Park, Y.H., Lee, C.R., Kim, Y.R. and Seok, Y.J. (2016) Glucose induces delocalization of a flagellar biosynthesis protein from the flagellated pole. *Mol. Microbiol.*, **101**, 795–808.
- Hayes, C.A., Dalia, T.N. and Dalia, A.B. (2017) Systematic genetic dissection of PTS in *Vibrio cholerae* uncovers a novel glucose transporter and a limited role for PTS during infection of a mammalian host. *Mol. Microbiol.*, **104**, 568–579.
- Kim, H.M., Yoon, C.K., Ham, H.I., Seok, Y.J. and Park, Y.H. (2018) Stimulation of *Vibrio vulnificus* Pyruvate Kinase in the Presence of Glucose to Cope With H₂O₂ Stress Generated by Its Competitors. *Front. Microbiol.*, **9**, 1112.
- Heo, K., Park, Y.H., Lee, K.A., Kim, J., Ham, H.I., Kim, B.G., Lee, W.J. and Seok, Y.J. (2019) Sugar-mediated regulation of a c-di-GMP phosphodiesterase in *Vibrio cholerae*. *Nat. Commun.*, **10**, 5358.
- Park, S., Yoon, J., Lee, C.R., Lee, J.Y., Kim, Y.R., Jang, K.S., Lee, K.H. and Seok, Y.J. (2019) Polar landmark protein HubP recruits flagella assembly protein FapA under glucose limitation in *Vibrio vulnificus*. *Mol. Microbiol.*, **112**, 266–279.
- Yoon, C.K., Kang, D., Kim, M.K. and Seok, Y.J. (2021) *Vibrio cholerae* FruR facilitates binding of RNA polymerase to the *fru* promoter in the presence of fructose 1-phosphate. *Nucleic Acids Res.*, **49**, 1397–1410.
- Yoon, J.H., Jeon, M.S., Eyun, S.I. and Seok, Y.J. (2022) Evidence for reciprocal evolution of the global repressor Mlc and its cognate phosphotransferase system sugar transporter. *Environ. Microbiol.*, **24**, 122–136.
- Lee, H.Y., Yoon, C.K., Cho, Y.J., Lee, J.W., Lee, K.A., Lee, W.J. and Seok, Y.J. (2022) A mannose-sensing AraC-type transcriptional activator regulates cell-cell aggregation of *Vibrio cholerae*. *NPJ Biofilms Microbiomes*, **8**, 65.
- Mandlik, A., Livny, J., Robins, W.P., Ritchie, J.M., Mekalanos, J.J. and Waldor, M.K. (2011) RNA-Seq-based monitoring of infection-linked changes in *Vibrio cholerae* gene expression. *Cell Host Microbe*, **10**, 165–174.
- Livny, J., Zhou, X., Mandlik, A., Hubbard, T., Davis, B.M. and Waldor, M.K. (2014) Comparative RNA-Seq based dissection of the regulatory networks and environmental stimuli underlying *Vibrio parahaemolyticus* gene expression during infection. *Nucleic Acids Res.*, **42**, 12212–12223.
- Jang, K.K., Lee, Z.W., Kim, B., Jung, Y.H., Han, H.J., Kim, M.H., Kim, B.S. and Choi, S.H. (2017) Identification and characterization of *Vibrio vulnificus* *plpA* encoding a phospholipase A2 essential for pathogenesis. *J. Biol. Chem.*, **292**, 17129–17143.
- Liu, Y., Liu, B., Xu, T., Wang, Q., Li, W., Wu, J., Zheng, X., Liu, B., Liu, R., Liu, X. *et al.* (2021) A fructose/H⁺ symporter controlled by a LacI-type regulator promotes survival of pandemic *Vibrio cholerae* in seawater. *Nat. Commun.*, **12**, 4649.
- Bag, J. (1974) Glucose inhibition of the transport and phosphoenolpyruvate-dependent phosphorylation of galactose and fructose in *Vibrio cholerae*. *J. Bacteriol.*, **118**, 764–767.
- Houot, L. and Watnick, P.I. (2008) A novel role for enzyme I of the *Vibrio cholerae* phosphoenolpyruvate phosphotransferase system in regulation of growth in a biofilm. *J. Bacteriol.*, **190**, 311–320.
- Kang, D., Ham, H.I., Lee, S.H., Cho, Y.J., Kim, Y.R., Yoon, C.K. and Seok, Y.J. (2021) Functional dissection of the phosphotransferase system provides insight into the prevalence of *Faecalibacterium prausnitzii* in the host intestinal environment. *Environ. Microbiol.*, **23**, 4726–4740.
- Park, Y.H., Lee, C.R., Choe, M. and Seok, Y.J. (2013) HPr antagonizes the anti- σ^{70} activity of Rsd in *Escherichia coli*. *Proc. Natl. Acad. Sci. USA*, **110**, 21142–21147.
- Choi, S.H., Lee, K.L., Shin, J.H., Cho, Y.B., Cha, S.S. and Roe, J.H. (2017) Zinc-dependent regulation of zinc import and export genes by Zur. *Nat. Commun.*, **8**, 15812.
- Ayala, J.C., Wang, H., Benitez, J.A. and Silva, A.J. (2018) Molecular basis for the differential expression of the global regulator VieA in *Vibrio cholerae* biotypes directed by H-NS, LeuO and quorum sensing. *Mol. Microbiol.*, **107**, 330–343.
- Lee, Z.W., Hwang, S.H., Choi, G., Jang, K.K., Lee, T.H., Chung, K.M., Kim, B.S. and Choi, S.H. (2020) A MARTX Toxin *rtxA* gene is controlled by host environmental signals through a CRP-Coordinated Regulatory Network in *Vibrio vulnificus*. *mBio*, **11**, e00723–20.
- Cho, B., Choi, J., Kim, R., Yun, J.N., Choi, Y., Lee, H.H. and Koh, J. (2021) Thermodynamic models for assembly of intrinsically disordered protein hubs with multiple interaction partners. *J. Am. Chem. Soc.*, **143**, 12509–12523.
- Heo, K., Lee, J.W., Jang, Y., Kwon, S., Lee, J., Seok, C., Ha, N.C. and Seok, Y.J. (2022) A pGpG-specific phosphodiesterase regulates cyclic di-GMP signaling in *Vibrio cholerae*. *J. Biol. Chem.*, **298**, 101626.
- An, Y.J., Kim, M.K., Song, J.M., Kang, M.H., Lee, Y.H. and Cha, S.S. (2015) Vapor batch crystallization and preliminary X-ray crystallographic analysis of a cold-active endo- β -1, 4-glucanase that was produced through the cold temperature protein expression. *Biodesign*, **3**, 138–142.
- Otwinowski, Z. and Minor, W. (1997) Processing of X-ray diffraction data collected in oscillation mode. *Methods Enzymol.*, **276**, 307–326.
- Schumacher, M.A., Allen, G.S., Diel, M., Seidel, G., Hillen, W. and Brennan, R.G. (2004) Structural basis for allosteric control of the transcription regulator CcpA by the phosphoprotein HPr-Ser46-P. *Cell*, **118**, 731–741.
- Liebschner, D., Afonine, P.V., Baker, M.L., Bunkoczi, G., Chen, V.B., Croll, T.I., Hintze, B., Hung, L.W., Jain, S., McCoy, A.J. *et al.* (2019) Macromolecular structure determination using X-rays, neutrons and

- electrons: recent developments in Phenix. *Acta Crystallogr. D Struct. Biol.*, **75**, 861–877.
38. Emsley, P. and Cowtan, K. (2004) Coot: model-building tools for molecular graphics. *Acta. Crystallogr. D Biol. Crystallogr.*, **60**, 2126–2132.
 39. Kornberg, H.L. (2001) Routes for fructose utilization by *Escherichia coli*. *J. Mol. Microbiol. Biotechnol.*, **3**, 355–359.
 40. Beck, C., Perry, S., Stoebel, D.M. and Liu, J.M. (2021) Cra and cAMP Receptor Protein Have Opposing Roles in the Regulation of *fruB* in *Vibrio cholerae*. *J. Bacteriol.*, **203**, e00241–21.
 41. Saier, M.H. Jr. and Ramseier, T.M. (1996) The catabolite repressor/activator (Cra) protein of enteric bacteria. *J. Bacteriol.*, **178**, 3411–3417.
 42. Feldheim, D., Chin, A., Nierva, C., Feucht, B., Cao, Y.W., Xu, Y.F., Sutrina, S. and Saier, M. (1990) Physiological consequences of the complete loss of phosphoryl-transfer proteins HPr and FPr of the phosphoenolpyruvate: sugar phosphotransferase system and analysis of fructose (*fru*) operon expression in *Salmonella typhimurium*. *J. Bacteriol.*, **172**, 5459–5469.
 43. Nam, T.W., Park, Y.H., Jeong, H.J., Ryu, S. and Seok, Y.J. (2005) Glucose repression of the *Escherichia coli* *sdhCDAB* operon, revisited: regulation by the CRP-cAMP complex. *Nucleic Acids Res.*, **33**, 6712–6722.
 44. Lund, P.A. and Brown, N.L. (1989) Regulation of transcription in *Escherichia coli* from the *mer* and *merR* promoters in the transposon Tn501. *J. Mol. Biol.*, **205**, 343–353.
 45. Chavarria, M., Santiago, C., Platero, R., Krell, T., Casasnovas, J.M. and de Lorenzo, V. (2011) Fructose 1-phosphate is the preferred effector of the metabolic regulator Cra of *Pseudomonas putida*. *J. Biol. Chem.*, **286**, 9351–9359.
 46. Chavarria, M., Durante-Rodriguez, G., Krell, T., Santiago, C., Brezovsky, J., Damborsky, J. and de Lorenzo, V. (2014) Fructose 1-phosphate is the one and only physiological effector of the Cra (FruR) regulator of *Pseudomonas putida*. *FEBS Open Bio.*, **4**, 377–386.
 47. Bley Folly, B., Ortega, A.D., Hubmann, G., Bonsing-Vedelaar, S., Wijma, H.J., van der Meulen, P., Miliias-Argeitis, A. and Heinemann, M. (2018) Assessment of the interaction between the flux-signaling metabolite fructose-1,6-bisphosphate and the bacterial transcription factors CggR and Cra. *Mol. Microbiol.*, **109**, 278–290.
 48. Ross, W., Ernst, A. and Gourse, R.L. (2001) Fine structure of *E. coli* RNA polymerase-promoter interactions: α subunit binding to the UP element minor groove. *Genes Dev.*, **15**, 491–506.
 49. Neetu, N., Katiki, M., Mahto, J.K., Sharma, M., Narayanan, A., Maity, S., Tomar, S., Ambatipudi, K., Sharma, A.K., Yernool, D. *et al.* (2021) Deciphering the enigma of missing DNA binding domain of LacI family transcription factors. *Arch. Biochem. Biophys.*, **713**, 109060.
 50. Peterkofsky, A., Wang, G., Garrett, D.S., Lee, B.R., Seok, Y.J. and Clore, G.M. (2001) Three-dimensional structures of protein-protein complexes in the *E. coli* PTS. *J. Mol. Microbiol. Biotechnol.*, **3**, 347–354.
 51. Park, Y.H., Um, S.H., Song, S., Seok, Y.J. and Ha, N.C. (2015) Structural basis for the sequestration of the anti- σ^{70} factor Rsd from σ^{70} by the histidine-containing phosphocarrier protein HPr. *Acta. Crystallogr. D Biol. Crystallogr.*, **71**, 1998–2008.
 52. Ha, J.H., Hauk, P., Cho, K., Eo, Y., Ma, X., Stephens, K., Cha, S., Jeong, M., Suh, J.Y., Sintim, H.O. *et al.* (2018) Evidence of link between quorum sensing and sugar metabolism in *Escherichia coli* revealed via cocrystal structures of LsrK and HPr. *Sci. Adv.*, **4**, eaar7063.
 53. Wray, L.V. Jr., Zalieckas, J.M. and Fisher, S.H. (2001) *Bacillus subtilis* glutamine synthetase controls gene expression through a protein-protein interaction with transcription factor TnrA. *Cell*, **107**, 427–435.
 54. Weickert, M.J. and Adhya, S. (1992) A family of bacterial regulators homologous to Gal and Lac repressors. *J. Biol. Chem.*, **267**, 15869–15874.
 55. Schumacher, M.A., Sprehe, M., Bartholomae, M., Hillen, W. and Brennan, R.G. (2011) Structures of carbon catabolite protein A-(HPr-Ser46-P) bound to diverse catabolite response element sites reveal the basis for high-affinity binding to degenerate DNA operators. *Nucleic Acids Res.*, **39**, 2931–2942.
 56. Mijakovic, I., Poncet, S., Galinier, A., Monedero, V., Fieulaine, S., Janin, J., Nessler, S., Marquez, J.A., Scheffzek, K., Hasenbein, S. *et al.* (2002) Pyrophosphate-producing protein dephosphorylation by HPr kinase/phosphorylase: a relic of early life? *Proc. Natl. Acad. Sci. USA*, **99**, 13442–13447.
 57. Jones, B.E., Dossanet, V., Küster, E., Hillen, W., Deutscher, J. and Klevit, R.E. (1997) Binding of the catabolite repressor protein CcpA to its DNA target is regulated by phosphorylation of its corepressor HPr. *J. Biol. Chem.*, **272**, 26530–26535.
 58. Henkin, T.M. (1996) The role of CcpA transcriptional regulator in carbon metabolism in *Bacillus subtilis*. *FEMS Microbiol. Lett.*, **135**, 9–15.
 59. Meinhardt, S., Manley Jr., Becker, N.A., Hessman, J.A., Maher, L.J. 3rd and Swint-Kruse, L. (2012) Novel insights from hybrid LacI/GalR proteins: family-wide functional attributes and biologically significant variation in transcription repression. *Nucleic Acids Res.*, **40**, 11139–11154.
 60. Chavarria, M., Fuhrer, T., Sauer, U., Pfluger-Grau, K. and de Lorenzo, V. (2013) Cra regulates the cross-talk between the two branches of the phosphoenolpyruvate : phosphotransferase system of *Pseudomonas putida*. *Environ. Microbiol.*, **15**, 121–132.
 61. Jang, C., Hui, S., Lu, W., Cowan, A.J., Morscher, R.J., Lee, G., Liu, W., Tesz, G.J., Birnbaum, M.J. and Rabinowitz, J.D. (2018) The Small Intestine Converts Dietary Fructose into Glucose and Organic Acids. *Cell Metab.*, **27**, 351–361.
 62. Douard, V. and Ferraris, R.P. (2013) The role of fructose transporters in diseases linked to excessive fructose intake. *J. Physiol.*, **591**, 401–414.
 63. Rohmer, L., Hocquet, D. and Miller, S.I. (2011) Are pathogenic bacteria just looking for food? Metabolism and microbial pathogenesis. *Trends Microbiol.*, **19**, 341–348.
 64. Shi, W., Zhang, B., Jiang, Y., Liu, C., Zhou, W., Chen, M., Yang, Y., Hu, Y. and Liu, B. (2021) Structural basis of copper-efflux-regulator-dependent transcription activation. *Iscience*, **24**, 102449.
 65. Yang, Y., Liu, C., Zhou, W., Shi, W., Chen, M., Zhang, B., Schatz, D.G., Hu, Y. and Liu, B. (2021) Structural visualization of transcription activated by a multidrug-sensing MerR family regulator. *Nat. Commun.*, **12**, 2702.
 66. Fang, C., Philips, S.J., Wu, X., Chen, K., Shi, J., Shen, L., Xu, J., Feng, Y., O'Halloran, T.V. and Zhang, Y. (2021) CueR activates transcription through a DNA distortion mechanism. *Nat. Chem. Biol.*, **17**, 57–64.
 67. Manneh-Roussel, J., Haycocks, J.R.J., Magan, A., Perez-Soto, N., Voelz, K., Camilli, A., Krachler, A.M. and Grainger, D.C. (2018) cAMP Receptor Protein Controls *Vibrio cholerae* Gene Expression in Response to Host Colonization. *mBio*, **9**, e00966–18.